Quantifying Statistical Interdependence, Part III: N > 2 Point Processes

LETTER **Communicated by Jonathan Victor**

Quantifying Statistical Interdependence, Part III: $N > 2$ Point Processes

Justin Dauwels
jdauwels@ntu.edu.sg
School of Electrical and Electronic Engineering, Nanyang Technological University, 639798 Singapore

Theophane Weber
theo_w@mit.edu
Operations Research Center, MIT, Cambridge, MA 02132, U.S.A.

François Vialatte
fvialatte@brain.riken.jp
Laboratory for Advanced Brain Signal Processing, RIKEN Brain Science Institute, Saitama 351-0198, Japan, and Laboratoire SIGMA, ESPCI ParisTech, 75231 Paris, France

Toshimitsu Musha
musha@bfl.co.jp
Brain Functions Laboratory, Yokohama 226-8510, Japan

Andrzej Cichocki
cia@brain.riken.jp
Laboratory for Advanced Brain Signal Processing, RIKEN Brain Science Institute, Saitama 351-0198, Japan

Stochastic event synchrony (SES) is a recently proposed family of similarity measures. First, "events" are extracted from the given signals; next, one tries to align events across the different time series. The better the alignment, the more similar the N time series are considered to be. The similarity measures quantify the reliability of the events (the fraction of "nonaligned" events) and the timing precision. So far, SES has been developed for pairs of one-dimensional (Part I) and multidimensional (Part II) point processes. In this letter (Part III), SES is extended from pairs of signals to $N > 2$ signals. The alignment and SES parameters are again determined through statistical inference, more specifically, by alternating two steps: (1) estimating the SES parameters from a given alignment and (2), with the resulting estimates, refining the alignment. The SES parameters are computed by maximum a posteriori (MAP) estimation (step 1), in analogy to the pairwise case. The alignment (step 2)

is solved by linear integer programming. In order to test the robustness and reliability of the proposed *N*-variate SES method, it is first applied to synthetic data. We show that *N*-variate SES results in more reliable estimates than bivariate SES. Next *N*-variate SES is applied to two problems in neuroscience: to quantify the firing reliability of Morris-Lecar neurons and to detect anomalies in EEG synchrony of patients with mild cognitive impairment. Those problems were also considered in Parts I and II, respectively. In both cases, the *N*-variate SES approach yields a more detailed analysis.

1 Introduction

Neural synchrony may play an important role in information processing in the brain. Although the details of this coding mechanism have not been fully revealed, it has been postulated that neural synchrony may be involved in cognition (Varela, Lachaux, Rodriguez, & Martinerie, 2001) and even in consciousness (Singer, 2001). The correlation between different brain signals has been studied intensively in recent years by both experimental neuroscientists (Abeles, Bergman, Margalit, & Vaadia, 1993; Womelsdorf et al., 2007) and computational neuroscientists (Amari, Nakahara, Wu, & Sakai, 2003) and also by neurologists. Indeed, various medical studies have reported that neurological diseases, such as Alzheimer's disease and epilepsy are related to perturbations in neural synchrony (Matsuda, 2001; Jeong, 2004).

Motivated by the intensified interest in neural synchrony, numerous researchers have developed and refined methods to quantify the synchrony between signals (Stam, 2005; Quiroga, Kraskov, Kreuz, & Grassberger, 2002; Pereda, Quiroga, & Bhattacharya, 2005; Toups, Fellous, Thomas, Sejnowski, & Tiesinga, 2011). In recent work, (Dauwels, Vialatte, Rutkowski, & Cichocki, 2008; Dauwels, Vialatte, Weber, & Cichocki, 2009a, 2009b), we have proposed a new family of synchrony measures referred to as stochastic event synchrony (SES); this class of measures is inspired by the Victor-Purpura distance metrics (Victor & Purpura, 1997). The basic idea is as follows. First, we extract "events" from the given time series; next, we try to align events from one time series with events from the other. The better the alignment, the more similar the time series are considered to be. We also quantify the timing jitter between matched ("coincident") events; the smaller the timing jitter, the larger the synchrony. SES thus considers two aspects of synchrony: reliability and timing precision. Those concepts were also recently considered in Toups et al. (2011), and they can be understood from an analogy. When you wait for a train at the station, the train may come, or it may not come at all; for example, it may be out of service due to some mechanical problem. If the train comes, it may or may not be on time. The former uncertainty is related to reliability, whereas the latter is related to precision.

So far, SES has been restricted to pairs of signals. In this letter, we extend SES from pairs of signals to $N > 2$ signals. The underlying principle is similar, but the inference algorithm to compute the SES parameters is fundamentally different. In bivariate SES (Dauwels, Vialatte et al., 2008, 2009a, 2009b), we applied the max-product algorithm to align pairs of sequences. We have implemented the max-product algorithm (and various refinements) for aligning $N > 2$ sequences as well; however, that approach unfortunately leads to inaccurate alignments, probably because N-wise alignment is substantially harder than pairwise alignment. As an alternative, we solve the N-wise alignment by integer linear programming, which yields optimal or near-optimal alignments at reasonable computational cost.

The extension from pairs of signals to $N > 2$ signals is nontrivial. In the following, we briefly touch on this issue. For $N = 2$, the problem of time series comparison is essentially that of finding an alignment between the time series. The alignment approach of Victor and Purpura (1997) was the inspiration for bivariate SES; we have shown in Dauwels et al. (2009a, 2009b) that the alignment between two time series (say, x_1 and x_2) is the same as finding an underlying time series v, which can then be transformed to x_1 and x_2 by a sequence of steps involving jittering the events, and insertions and deletions. Quantifying the distance between x_1 and x_2 is equivalent to finding a v that minimizes some combination of $d(x_1, v)$ and $d(x_2, v)$. By making the combination rule for these two distances accelerating (such as a root mean square), one can ensure that v is in the middle of x_1 and x_2. Comparing x_1 with x_2 is equivalent to finding a hidden consensus process v that can generate both x_1 with x_2. Finding the v interprets the similarity of x_1 and x_2 in terms of a consensus that they both represent, but it is not necessary to find v to quantify this similarity, since it can also be expressed as an alignment, without an explicit v.

For $N = 3$, one can attempt to jointly minimize some combination of $d(x_1, v)$, $d(x_2, v)$, and $d(x_3, v)$ without attempting to find an underlying v. Or one can attempt to find a single v for which some combination of $d(x_1, v)$, $d(x_2, v)$, and $d(x_3, v)$ is smallest.

Finally, for $N > 3$, there is at least one other possibility: the point process might be generated by two or more hidden processes. This can first happen at $N = 4$, with two hidden processes, say v and w, for which the distances $d(x_1, v), d(x_2, v), d(x_3, w), d(x_4, w)$ have a lower total than the distance from any single v to all four of the observations x_1, x_2, x_3, and x_4. In other words, for $N > 3$, the problem of finding multivariate similarity is generally not the same as finding the single underlying consensus process.

In summary, there are at least three kinds of definitions of synchrony and similarity:

1. A definition based on the $N(N-1)/2$ distances $d(x_i, x_j)$ between pairs of observed processes

2. A definition based on finding a consensus process v, which minimizes the N distances $d(x_i, v)$
3. A definition based on finding multiple hidden processes

For $N = 2$, these definitions are identical. For $N = 3$, the second and third are identical but differ from the first. For $N > 3$, all three definitions are distinct. In this letter, we consider the second definition: the N point processes are generated from a (hidden) consensus process v. In future work, we will extend N-variate SES to multiple hidden processes.

Stochastic event synchrony (SES) is applicable to any kind of time series (e.g., finance, oceanography, seismology). We consider here neural spike trains and electroencephalograms (EEG). More specifically, we use the SES method to quantify the reliability of Morris-Lecar neurons and predict mild cognitive impairment (MCI) from electroencephalograms. We also considered those problems in Part I (Dauwels et al., 2009a) and Part II (Dauwels et al., 2009b), respectively.

This letter is organized as follows. In the next section, we explain how SES can be extended from pairs of point processes to $N > 2$ point processes. We describe the underlying statistical model in section 3 and outline our inference method in section 4.[1] We consider various extensions of our statistical model in section 5. We investigate the robustness and reliability of the SES inference method by means of synthetic data in section 6. We use SES to quantify the reliability of Morris-Lecar neurons section 7 and detect abnormalities in the EEG synchrony of MCI disease patients in section 8. We offer some concluding remarks in section 9.

Readers who are less interested in the technical details may wish to read section 2, where the general idea is outlined, and sections 7 and 8, where two applications are discussed. Those sections can be read independently of the more technical sections 3 and 4.

2 Principle

Suppose that we are given $N > 2$ continuous-time signals (e.g., EEG signals recorded from different channels), and we wish to determine the similarity of those signals. In Dauwels et al. (2009b), we considered pairs of signals ($N = 2$). Although the extension to $N > 2$ may seem straightforward, it leads to a combinatorial problem that is much harder. In the following, we closely follow the setting and notation of Dauwels et al. (2009b).

As a first step, we extract point processes from those $N > 2$ signals, which may be achieved in various ways. As an example, we generate point processes in the time-frequency domain. First, the time frequency (wavelet) transform of each signal is computed in a frequency band $f \in [f_{\min}, f_{\max}]$.

[1] An implementation of N-variate SES for one-dimensional and multidimensional point processes is available online at http://www.dauwels.com/SESToolbox/SES.html.

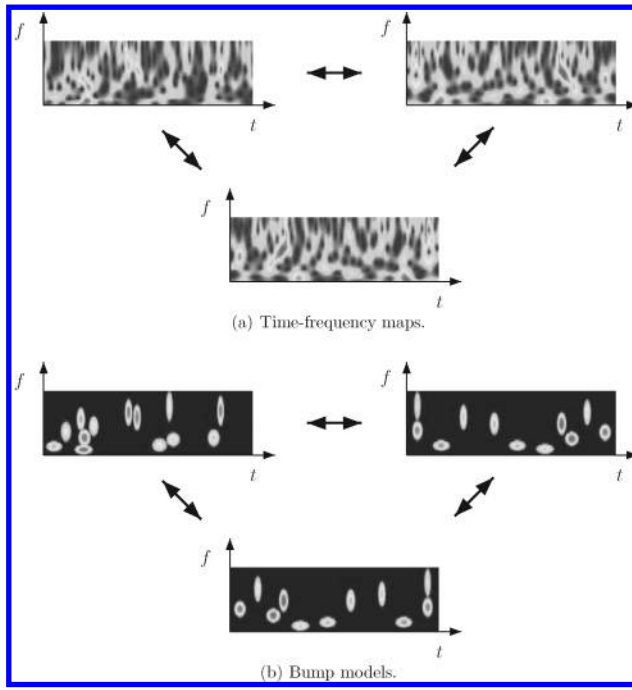

Figure 1: Similarity of three EEG signals ($N = 3$). From their time-frequency transforms (top), one extracts two-dimensional point processes (bump models; bottom), which are then aligned.

Next, those maps are approximated as a sum of half-ellipsoid basis functions, referred to as bumps (see Figure 1 and Vialatte et al., 2007). Each bump is described by five parameters: time t, frequency f, width Δt, height Δf, and amplitude w. The resulting bump models represent the most prominent oscillatory activity in the signals at hand. This activity may correspond to various physical or biological phenomena. For example, oscillatory events in EEG and other brain signals are believed to occur when assemblies of neurons are spiking in synchrony (Buzsáki, 2006; Nunez & Srinivasan, 2006). In the following, we develop N-variate SES for bump models. In this setting, SES quantifies the synchronous interplay between oscillatory patterns in $N > 2$ given signals, while it ignores the other components in those signals (the background activity). In contrast, classical synchrony measures such as amplitude or phase synchrony are computed from the entire signal; they make no distinction between oscillatory components and the background activity. As a consequence, SES captures alternative aspects of similarity and hence provides complementary information about synchrony.

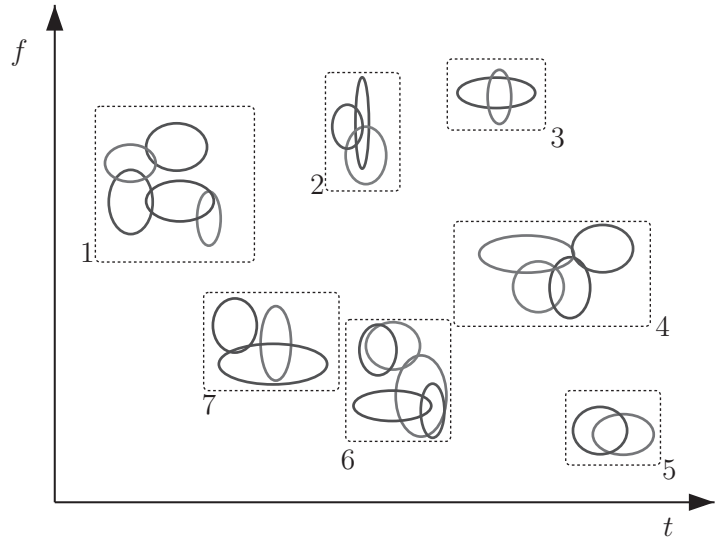

Figure 2: Five bump models overlaid on top of each other ($N = 5$). The dashed boxes indicate clusters. The average offset between the bumps is close to zero.

Besides bump models, SES may be applied to other sparse representations of signals. Moreover, the point processes may be defined in spaces other than the time-frequency plane; for example, they may occur in two-dimensional space (e.g., images), space frequency (e.g., wavelet image coding), or space time (e.g., movies). Such extensions may straightforwardly be derived from the example of bump models (we refer to section 5 and Dauwels et al., 2009b, for more details).

It is also noteworthy that the events in the point processes may be labeled by discrete tags. For example, in multineuronal recordings, the labels would correspond to the neurons of origin. More generally, the labels may correspond to the sites or processes of origin. SES may then be applied to the point processes associated with each label, and it would quantify the coupling between the different sites (e.g., neurons).

We now consider the central question: How can we quantify the similarity of $N > 2$ point processes defined on a space S? Let us consider the example of bump models (see Figures 1 and 2). Intuitively speaking, N bump models $(x_i)_{i=1,2,\ldots,N}$ may be considered well synchronized if bumps appear in (almost) all bump models simultaneously, apart from a constant offset in time and frequency and a small amount of jitter in time and frequency. If one overlays N well-synchronized bump models and removes the potential average offsets in time and frequency (denoted by δ_{ti} and δ_{fi} respectively, for $i = 1, 2, \ldots, N$), bumps naturally appear in clusters that contain precisely

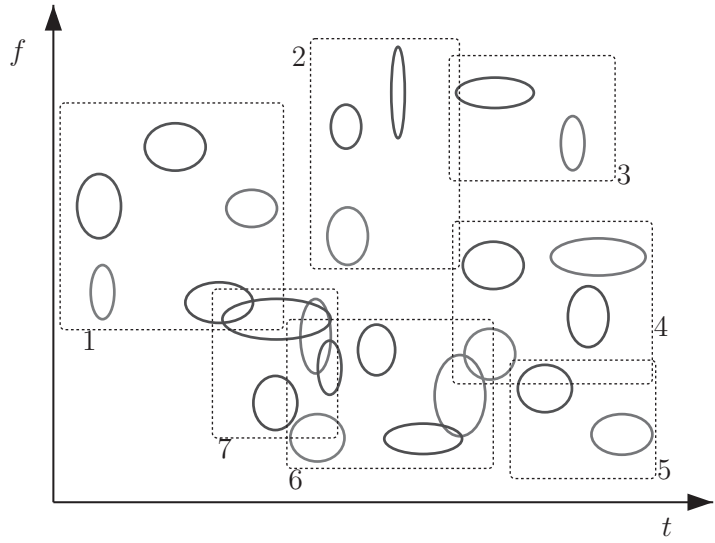

Figure 3: Five bump models overlaid on top of each other ($N = 5$). The dashed boxes indicate clusters. The average offset between the bumps is nonzero.

one bump from all (or almost all) bump models, as illustrated in Figure 2 for $N = 5$. In that example, clusters 1 and 6 contain bumps from all five bump models x_i, clusters 2 and 7 contain bumps from three bump models, clusters 3 and 5 contain bumps from two bump models, and cluster 4 contains bumps from four bump models. In general, the average offset in time and frequency between the bumps is not necessarily zero (as illustrated in Figure 3), and it may be harder to recognize the different clusters. The algorithm developed in this letter is able to extract such clusters, even in the general case of nonzero average offsets in time and frequency (as in Figure 3).

If the point processes are well synchronized, almost all clusters contain (close to) N bumps, specifically, one bump from each (or almost each) of the N bump models. Therefore, an important similarity statistics is the average number of events per cluster or, more generally, the statistical distribution of the number of events per cluster. Moreover, as in the pairwise case (Dauwels et al., 2009a, 2009b), one can quantify how well the bumps are aligned within each cluster by computing the jitter s_{ti} and s_{fi} in time and frequency, respectively, for $i = 1, 2, \ldots, N$.

More generally, N point processes on a space S may be considered similar if events appear in clusters with (close to) N events and with small dispersion (computed by the distance measure on S). Those clusters may appear only after certain transformations have been applied, such as translation

(to eliminate offsets as in Figure 3), rotation, and scaling. In other words, N point processes are considered similar if they can be transformed into each other by a few operations, including deletions and insertions, small random perturbations, and transformations such as translation, rotation, and scaling.

Let us now return to bump models. We determine the SES parameters δ_{ti}, δ_{fi}, s_{ti}, and s_{fi} ($i = 1, 2, \ldots, N$) and the event clusters by statistical inference, along the lines of the pairwise case (Dauwels et al., 2009a, 2009b). We start by constructing a statistical model that captures the relation between the N bump models. That statistical model contains the SES parameters besides variables related to the alignment of the different bumps. Next, we perform inference in that statistical model, resulting in estimates for the SES parameters and clusters. More concretely, we apply cyclic maximization, as in the pairwise case.

In section 3, we outline our statistical model; in section 4, we describe how we conduct inference in that statistical model.

3 Statistical Model

3.1 Casual Description. The intuitive concept of similarity outlined in section 2 may readily be translated into a generative stochastic model. In that model, the N point processes x_i are treated as independent noisy observations of a hidden process v. The observed sequences $(x_i)_{i=1,\ldots,N}$ are obtained from v by the following four-step procedure:

1. Copy. Generate N copies of the hidden point process v.
2. Deletion. Delete some of the copied events.
3. Perturbation. Shift the remaining copies over $(\delta_{ti}, \delta_{fi})_{i=1,\ldots,N}$, and randomly perturb the positions, with variance $(s_i)_{i=1,\ldots,N} = (s_{ti}, s_{fi})_{i=1,\ldots,N}$, amounting to the N point processes $(x_i)_{i=1,\ldots,N}$.
4. Insertion. Additional events are inserted (background events) that are unrelated to the hidden point process v and are modeled as mutually independent.

As a result, each sequence x_i consists of noisy copies of hidden events (generated by steps 1 to 3), besides background events (generated by step 4). The noisy copies are related to each other through the hidden events v, whereas the background events are all independent of each other. The point processes x_i may be considered well synchronized if there are only few deletions (see step 2) and insertions (step 4) and if the events of x_i are close to the corresponding hidden events (see step 3), apart from offsets $(\delta_{ti}, \delta_{fi})_{i=1,\ldots,N}$. Figure 4 illustrates a generative process that results in the bump models of Figure 3. More generally, as we pointed out in the previous section, one may include other transformations in the perturbation step besides translation over $(\delta_{ti}, \delta_{fi})_{i=1,\ldots,N}$, such as rotation and scaling.

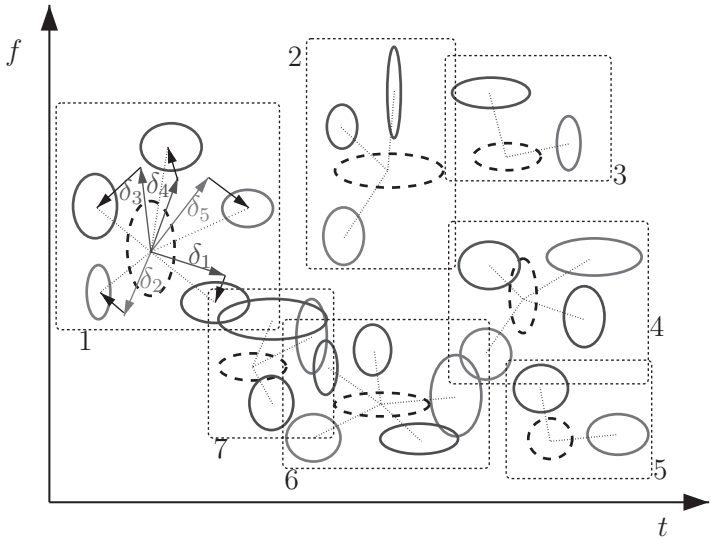

Figure 4: Generative model for the $N = 5$ bump models $(x_i)_{i=1,\ldots,N}$ of Figure 3. One first generates a hidden bump model v, indicated in dashed lines. Next, one makes $N = 5$ identical copies of v and shifts those over $(\delta_i)_{i=1,\ldots,N} = (\delta_{ti}, \delta_{fi})_{i=1,\ldots,N}$, as indicated by the arrows (labeled δ_i) in cluster 1. The resulting events are then slightly shifted, with variance $(s_i)_{i=1,\ldots,N} = (s_{ti}, s_{fi})_{i=1,\ldots,N}$, as indicated by the other arrows in cluster 1. Finally, some of those events are deleted (with probability p_d), resulting in the bump models $(x_i)_{i=1,\ldots,N}$. For example, two events are deleted in cluster 2.

Some readers may wonder why insertions need to be modeled explicitly. Indeed, inserting an event is equivalent to adding a hidden event with N noisy copies, followed by $N-1$ deletions. In this way, the SES models for pairs of point processes (Parts I and II) are able to capture insertions, even though they are not modeled explicitly (Dauwels et al., 2009a, 2009b). However, for large N (e.g., $N > 10$), the cost of an insertion becomes prohibitively large (due to the $N-1$ deletions), and as a consequence, the statistical model no longer captures insertions. The inserted event will be grouped with other events, leading to incorrect clusters. Therefore, it becomes necessary to model insertions explicitly. As an illustration, Figure 11a shows several event clusters in addition to background events (indicated by hexagons). More information on this application can be found in section 7. Note that insertions are also explicitly modeled in the Victor and Purpura (1997) distance metrics, which were the source of inspiration for SES.

3.2 Formal Description. We now describe the underlying stochastic model in more detail. We refer to Table 1 for a summary of all relevant variables and parameters. For convenience, we introduce the following notation. The length of the point process x_i is denoted by L_i (with $i = 1, 2, \ldots, N$). The individual events of point process x_i are denoted by x_{ij} (with $i = 1, 2, \ldots, N$ and $j = 1, \ldots, L_i$). The occurrence time and frequency of those events are referred to as t_{ij} and f_{ij}, respectively. Moreover, we will use the notation $\delta_i = (\delta_{ti}, \delta_{fi})$, $s_i = (s_{ti}, s_{fi})$, $\theta_i = (\delta_i, s_i)$ (with $i = 1, 2, \ldots, N$), and $\theta = (\theta_1, \theta_2, \ldots, \theta_N)$.

The hidden process $v = \{v_1, \ldots, v_\ell\}$, which is the source of all events in $x_1, x_2, \ldots x_N$ (besides the background events; see step 4), is modeled as follows. The number ℓ of points in v is geometrically distributed with parameter $\lambda \operatorname{vol}(S)$:

$$p(\ell) = (1 - \lambda \operatorname{vol}(S))\big(\lambda \operatorname{vol}(S)\big)^{\ell}, \tag{3.1}$$

where $\operatorname{vol}(S)$ is the multidimensional volume of set S. (We motivate this choice of prior in Part I (Dauwels et al., 2009a, 2009b).) In the particular case of bump models in the time-frequency domain, the space S is defined as

$$S = \{(t, f) : t \in [t_{\min}, t_{\max}] \quad \text{and} \quad f \in [f_{\min}, f_{\max}]\}, \tag{3.2}$$

and therefore

$$\operatorname{vol}(S) = (t_{\max} - t_{\min})(f_{\max} - f_{\min}). \tag{3.3}$$

Each point v_k for $k = 1, \ldots, \ell$ is uniformly distributed in S:

$$p(\tilde{t}, \tilde{f}|\ell) = \operatorname{vol}(S)^{-\ell}, \tag{3.4}$$

where $\tilde{t}$ and $\tilde{f}$ are the positions of the hidden events $(v_k)_{k=1,\ldots,\ell}$ in time and frequency, respectively. The amplitudes, widths, and heights of the bumps v_k are independently and identically distributed according to priors p_w, $p_{\Delta t}$, and $p_{\Delta f}$, respectively. In the following, we will discard those priors since they are irrelevant. With those choices, the prior of the hidden process v equals

$$p(v, \ell) = p(\ell)p(v|\ell) \propto (1 - \lambda \operatorname{vol}(S))\lambda^{\ell}, \tag{3.5}$$

where the priors for the amplitudes, widths, and heights of the bumps v_k have been discarded for convenience.

From the hidden process v, the point processes $(x_i)_{i=1,\ldots,N}$ are generated as follows (see Figure 4). We first generate N identical copies of v. Next,

Table 1: List of Variables and Parameters Associated with Models $p(x, c, v, \theta, \ell)$, Equation 3.16; $p(x, c, \theta)$, Equations 3.23 and 4.12; and $p(x, b, e, \theta)$, Equations 4.12 and 4.18.

Symbol	Explanation
$(x_i)_{i=1,2,\ldots,N}$	N given bump models
L_i	Length of x_i
L^{tot}	Total number of bumps in the N models $(x_i)_{i=1,2,\ldots,N}$
x_{ij}	jth bump in bump model x_i
t_{ij}	Occurrence time of x_{ij}
f_{ij}	Frequency of x_{ij}
δ_{ti} and δ_{fi}	Average offset in time and frequency for bump model x_i
s_{ti} and s_{fi}	Jitter in time and frequency for bump model x_i
p_d	Deletion probability
v	Hidden bump model from which the observed bump models $(x_i)_{i=1,2,\ldots,N}$ are generated
ℓ	Length of v
c_{ij}	$c_{ij} = 0$ if x_{ij} is a background event, otherwise index of event in v that generated x_{ij}
$\mathcal{C}_k$	Set of n_k copies of v_k (see equation 3.13)
$\mathcal{I}_k$	Index set of $\mathcal{C}_k$ (see equation 3.13)
$\mathcal{K}$	Index set of bump clusters of size $n_k > 1$ (see equation 3.12)
L	Number of bump clusters, that is, number of hidden events v_k with at least one copy ($n_k > 0$)
ρ	Fraction of missing bumps in the clusters
$\tilde{v}$	Background events in $(x_i)_{i=1,2,\ldots,N}$
$\tilde{\ell}$	Length of $\tilde{v}$
χ	Fraction of background events in $(x_i)_{i=1,2,\ldots,N}$
d_0	Cost associated with a cluster/exemplar (see equation 3.25)
d_0	Cost associated with a background event (see equation 3.26)
$d(t_{ij}, f_{ij})$	Cost associated with an event x_{ij} that belongs to a nontrivial cluster (see equation 3.27)
$d(t_{ij}, f_{ij}, t_{i'j'}, f_{i'j'})$	Cost associated with an event x_{ij} that belongs to exemplar $x_{i'j'}$ (see equation 4.17)
b_k	Equal to one iff cluster k is nonempty ($n_k > 0$ and $k = 1, 2, \ldots, L^{\text{tot}}$), otherwise zero
b_{ijk}	Equal to one iff the x_{ij} belongs to cluster k, i.e., $c_{ij} = k$, otherwise zero
b_{ij}	Equal to one iff x_{ij} is an exemplar, otherwise zero
$b_{iji'j'}$	Equal to one iff x_{ij} is associated with exemplar $x_{i'j'}$, otherwise zero
e_{ij}	Equal to one iff x_{ij} is a background event, otherwise zero

the amplitudes, widths, and heights of the bumps are replaced by random independent draws from priors p_w, $p_{\Delta t}$, and $p_{\Delta f}$, respectively. Again, those priors are irrelevant for what follows, and we will omit them. Next, each event is removed with probability p_d ("deletion"), independent of the other events. The probability mass associated with the (remaining) n_k copies of $(v_k)_{k=1,\ldots,\ell}$ is given by

$$p(n_k) = p_d^{N-n_k}(1-p_d)^{n_k}. \tag{3.6}$$

We will need the product of $p(n_k)$ for $k = 1, \ldots, \ell$:

$$\prod_{k=1}^{\ell} p(n_k) = p_d^{N\ell - L^{\text{tot}}}(1-p_d)^{L^{\text{tot}}}, \tag{3.7}$$

where L^{tot} is the total number of events in the N point processes $(x_i)_{i=1,\ldots,N}$:

$$L^{\text{tot}} = \sum_{i=1}^{N} L_i. \tag{3.8}$$

At last, the resulting N sequences are shifted over $(\delta_i)_{i=1,\ldots,N} = (\delta_{ti}, \delta_{fi})_{i=1,\ldots,N}$, and the occurrence times and frequencies are slightly perturbed, resulting in the sequences $(x_i)_{i=1,\ldots,N}$. As we pointed out earlier, there might be a nontrivial timing and frequency offset between the bump models (see Figures 3 and 4). The parameters $(\delta_{ti}, \delta_{fi})$ are introduced in the model to account for such offsets. The offsets between v and $(x_i)_{i=1,\ldots,N}$ may be modeled as bivariate gaussian random variables with mean vectors $(\delta_{ti}, \delta_{fi})$ and diagonal nonisotropic covariance matrices $V_i = \text{diag}(s_{ti}, s_{fi})$. It is reasonable to assume that the offsets in time are independent of the offsets in frequency, and vice versa. Therefore, we use diagonal matrices V_i. Statistical dependencies between the perturbations in time and frequency may be modeled by nondiagonal covariance matrices V_i. Such extensions are straightforward, and we do not consider them here.

We adopt the improper priors $p(\delta_{ti}) = 1 = p(\delta_{fi})$ for $(\delta_{ti})_{i=1,\ldots,N}$ and $(\delta_{fi})_{i=1,\ldots,N}$ respectively, and conjugate priors for s_{ti} and s_{fi}, that is, scaled inverse chisquare distributions:

$$p(s_{ti}) = \frac{(s_{t0}\nu_t/2)^{\nu_t/2}}{\Gamma(\nu_t/2)} \frac{e^{-\nu_t s_{t0}/2s_{ti}}}{s_{ti}^{1+\nu_t/2}}, \tag{3.9}$$

$$p(s_{fi}) = \frac{(s_{f0}\nu_f/2)^{\nu_f/2}}{\Gamma(\nu_f/2)} \frac{e^{-\nu_f s_{f0}/2s_{fi}}}{s_{fi}^{1+\nu_f/2}}, \tag{3.10}$$

where ν_t and ν_f are the degrees of freedom, s_{t0} and s_{f0} are the width of the scaled inverse chi square distributions, and $\Gamma(x)$ is the gamma function.

In Dauwels et al. (2009b), we normalized the parameters (δ_t, s_t) and (δ_f, s_f) by the width and height of the bumps, respectively, in order to take the size of the bumps into account. For simplicity, we will discard such normalization factors in the following. They can easily be incorporated in the statistical model, and we briefly address this issue in section 5.

It is also noteworthy that in Dauwels et al. (2009b), the variance of the time and frequency perturbations in the generative process is defined as $s_t/2$ and $s_f/2$, respectively (instead of s_t and s_f), so that the variance between the two observed sequences x_1 and x_2 is given by s_t and s_f. Therefore, when comparing results from bivariate and N-variate SES, a factor of two needs to be taken into account.

For later convenience, we introduce some more notation. We denote by $v_{c_{ij}}$ the hidden event that generated x_{ij} (the jth event in point process x_i). The function c is hence a clustering function that groups the events x_{ij} into different clusters. Since there is at most one event from point process i in cluster k, the clustering function c fulfills the constraints

$$\sum_{j=1}^{L_i} \delta\big[c_{ij} - k\big] \leq 1, \forall i, k. \tag{3.11}$$

Note that certain hidden events $(v_k)_{k=1,\ldots,\ell}$ may not have any copies, since all N copies may have been deleted. Therefore, the function c does not necessarily take ℓ different values. Without loss of generality, we will assume that c takes values in $\{1, 2, \ldots, L\}$, where L is the number of clusters and $0 \leq L \leq \ell$. Note that the number L of clusters is at most L^{tot}, that is, the total number of events; this maximum number occurs when each event is a cluster, and hence all clusters are of size 1. With this definition of L, the number of copies $n_1, \ldots, n_L$ are nonzero, whereas $n_{L+1} = n_{L+2} = \cdots = n_\ell = 0$. We introduce the index set $\mathcal{K}$ of clusters with $n_k > 1$:

$$\mathcal{K} = \{k \in \{1, 2, \ldots, L\} : n_k > 1\}. \tag{3.12}$$

We denote by $\mathcal{C}_k$ the set of n_k copies of v_k and denote its index set by $\mathcal{I}_k$:

$$\mathcal{C}_k = \{x_{ij} : c_{ij} = k\} \text{ and } \mathcal{I}_k = \{(i, j) : c_{ij} = k\}. \tag{3.13}$$

The fraction ρ of missing events in the clusters can be computed as

$$\rho = 1 - \frac{\sum_{k=1}^{L} n_k}{LN} = 1 - \frac{\bar{n}}{N}, \tag{3.14}$$

where $\bar{n}$ is the average number of events per cluster. Another important statistics is the distribution $(p_j)_{j=1}^{N}$ of the number of events per cluster:

$$p_j = \frac{\sum_{k=1}^{L} \delta[n_k - j]}{L}, \quad j = 1, 2, \ldots, N. \tag{3.15}$$

In this notation, the overall probabilistic model may be written as

$$p(x, c, v, \theta, \ell) \propto p(s_t)p(s_f)(1 - \lambda \operatorname{vol}(S))(\lambda\, p_d^N)^{\ell} p_d^{-L^{\mathrm{tot}}} (1 - p_d)^{L^{\mathrm{tot}}}$$
$$\cdot \prod_{i=1}^{N} \prod_{j=1}^{L_i} \mathcal{N}\big(t_{ij} - \tilde{t}_{c_{ij}}; \delta_{ti}, s_{ti}\big)\, \mathcal{N}\big(f_{ij} - \tilde{f}_{c_{ij}}; \delta_{fi}, s_{fi}\big). \tag{3.16}$$

Note that the parameters N, $(L_i)_{i=1,\ldots,N}$ and L^{tot} are fixed for given point processes. Likewise, for given clustering c, the parameters L and $(n_k)_{k=1,\ldots,L}$ are fixed. The total number of deletions is given by $L^{\mathrm{del,tot}} = N\ell - L^{\mathrm{tot}}$. The number of hidden events v_k without copies is given by $L^{\mathrm{del}} = \ell - L$.

As in Parts I and II, we can marginalize the statistical model $p(x, c, v, \theta, \ell)$ *analytically* with regard to v and ℓ (Dauwels et al., 2009a, 2009b), resulting in $p(x, c, \theta)$ (see appendix A):

$$p(x, c, \theta) \propto \gamma\, \beta^{NL} p(s_t)p(s_f)$$
$$\cdot \prod_{k \in \mathcal{K}} \prod_{(i,j) \in \mathcal{I}_k} \mathcal{N}\big(t_{ij} - \bar{t}_k; \delta_{ti}, s_{ti}\big)\, \mathcal{N}\big(f_{ij} - \bar{f}_k; \delta_{fi}, s_{fi}\big), \tag{3.17}$$

where

$$\bar{t}_k = \frac{\sum_{(i,j) \in \mathcal{I}_k} w_{ti}(t_{ij} - \delta_{ti})}{\sum_{(i,j) \in \mathcal{I}_k} w_{ti}}, \tag{3.18}$$

$$\bar{f}_k = \frac{\sum_{(i,j) \in \mathcal{I}_k} w_{fi}(f_{ij} - \delta_{fi})}{\sum_{(i,j) \in \mathcal{I}_k} w_{fi}}, \tag{3.19}$$

with $w_{ti} = s_{ti}^{-1}$ and $w_{fi} = s_{fi}^{-1}$. Interestingly, the parameters $(\bar{t}_k, \bar{f}_k)$ may be interpreted as the coordinates of the center of the n_k copies associated with v_k (see Figure 5 b); in other words, those n_k copies may be viewed as a cluster of events whose center is located at $(\bar{t}_k, \bar{f}_k)$. As can easily be shown, the latter parameters are also the maximum likelihood (ML) estimates of the time and frequency of the hidden event v_k, when the copies of v_k and the parameters

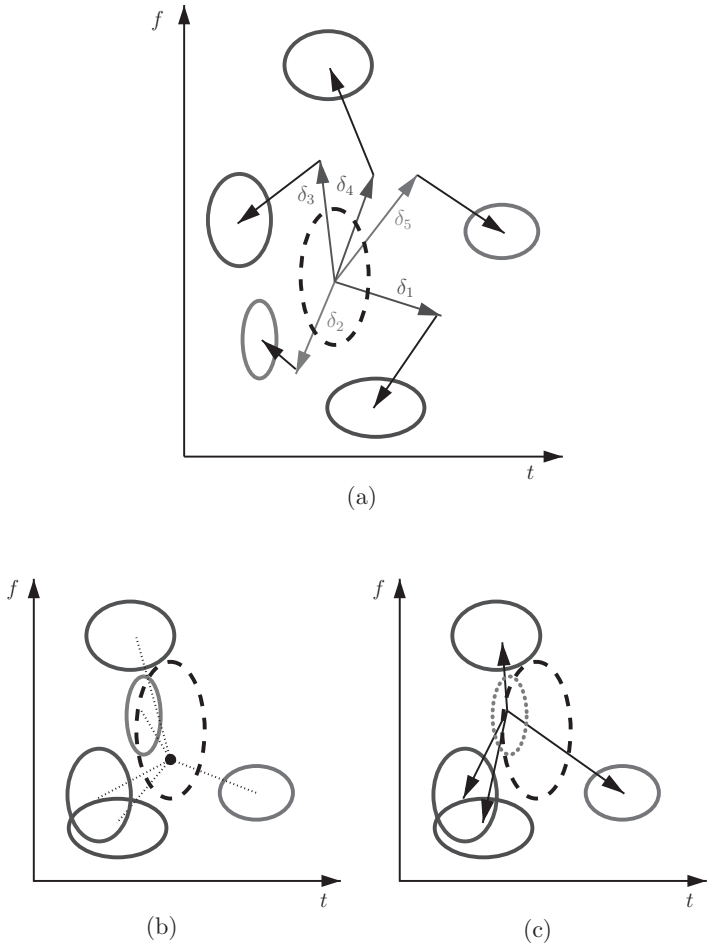

Figure 5: Exemplar representation. A cluster with five events, generated from a hidden event (dashed lines). For clarity, we have eliminated the offsets δ_i in *b* and *c*. The exemplar is marked in dotted lines in *c*. (a) Hidden event v_k (dashed line) and its five "noisy" copies. The arrows indicate the systematic offsets (δ_i) and random offsets. (b) For the sake of clarity, the offsets δ_i (see *a*) have been eliminated. The dot corresponds to the center of the five events (see equations 3.28 and 3.29), and the dotted lines indicate the distances $d(t_{ij}, f_{ij})$, equation 3.27. (c) After eliminating the offsets δ_i, event 2 (dotted) lies the closest to the hidden event (dashed), and it serves as exemplar. The arrows indicate the distances $d(t_{ij}, f_{ij}, t_{i'j'}, f_{i'j'})$ (see equation 4.17).

(δ_i, s_i) are given $(i = 1, 2 \ldots, N)$. In practice, the latter are usually not given, and therefore the coordinates $\bar{t}_k$ and $\bar{f}_k$ depend on how the events x_{ij} are assigned to hidden events v_k; in other words, those parameters depend on the clustering c.

The parameters β and γ in equation 3.17 are defined as

$$\beta = p_d \sqrt[N]{\lambda} \tag{3.20}$$

and

$$\gamma = \left(p_d^{-1}(1 - p_d)\right)^{L^{\text{tot}}} (1 - \lambda \text{vol}(S)) \frac{1}{1 - \lambda \text{vol}(S) p_d^N}. \tag{3.21}$$

Note that we defined similar parameters γ and β in Parts I and II (Dauwels et al. 2009a, 2009b); the N-variate statistical model, equation 3.17, is a natural extension of the pairwise statistical models of Dauwels et al., (2009a, 2009b). The constant γ does not depend on c or the SES parameters δ_i and s_i (with $i = 1, \ldots, N$), and therefore, it is irrelevant for estimating the latter parameters and the clusters. We will discard γ in the following.

So far, we have not yet taken background events into account. They can be modeled as follows. Besides the hidden process v, we generate the background events as a point process $\tilde{v}$ of length $\tilde{\ell}$. We define the prior $p(\tilde{v}, \tilde{\ell})$ similarly as $p(v, \ell)$ (see equation 3.5):

$$p(\tilde{v}, \tilde{\ell}) = p(\tilde{\ell}) p(\tilde{v}|\tilde{\ell}) \propto (1 - \tilde{\lambda} \, \text{vol}(S)) \tilde{\lambda}^{\tilde{\ell}}. \tag{3.22}$$

As a result, some of the events x are generated from v (according to steps 1–3), and the other events (background events) are the process $\tilde{v}$. We denote by χ the fraction of background events in x. To account for the background events, we now assume that c takes values in $\{0, 1, 2, \ldots, L\}$, where $c_{ij} = 0$ iff x_{ij} is a background event. From a given clustering function c, we can easily infer the background events (and hence also $\tilde{\ell}$). An important statistics is the fraction χ of background events, which can also easily be computed from c.

We can include background events in statistical model 3.17 by multiplying it with the prior $p(\tilde{v}, \tilde{\ell})$, equation 3.22, resulting in

$$\begin{aligned} p(x, c, \theta) &\propto \beta^{NL} \tilde{\beta}^{\tilde{\ell}} p(s_t) p(s_f) \\ &\cdot \prod_{k \in \mathcal{K}} \prod_{(i,j) \in \mathcal{I}_k} \mathcal{N}\left(t_{ij} - \bar{t}_k; \delta_{ti}, s_{ti}\right) \mathcal{N}\left(f_{ij} - \bar{f}_k; \delta_{fi}, s_{fi}\right), \end{aligned} \tag{3.23}$$

where the parameter $\tilde{\beta} = \tilde{\lambda}$ (see equation 3.20).

The exponent of β and $\tilde{\beta}$ in equation 3.23 clearly depends on c, and as a result, the parameters β and $\tilde{\beta}$ affect the inference of c and the SES parameters. As in Parts I and II, we will interpret those parameters in terms of cost functions; the expressions $\log \beta$ and $\log \tilde{\beta}$ are part of the cost associated with each cluster and background event, respectively. In all our experiments, we found that the setting $\tilde{\beta} = 10^{-20}$ yields satisfactory results.

3.3 Interpretation in Terms of Cost Functions. We can gain additional insight by considering the logarithm of statistical model 3.23,

$$\begin{aligned} -\log p(x, c, \theta) = &-\log p(s_t) - \log p(s_f) - LN \log \beta - \tilde{\ell} \log \tilde{\beta} \\ &+ \sum_{k \in \mathcal{K}} \sum_{(i,j) \in \mathcal{I}_k} \left(\frac{1}{2} \log 2\pi s_{ti} + \frac{1}{2s_{ti}} (t_{ij} - \bar{t}_k - \delta_{ti})^2 \right. \\ &\left. + \frac{1}{2} \log 2\pi s_{fi} + \frac{1}{2s_{fi}} (f_{ij} - \bar{f}_k - \delta_{fi})^2 \right) + \zeta, \end{aligned} \tag{3.24}$$

where ζ is an irrelevant constant. Expression 3.24 may be considered as a cost function that associates certain costs with each event and cluster; we provided a similar viewpoint in Parts I and II (Dauwels et al., 2009a, 2009b). The unit cost d_0 associated with each of the L clusters is given by

$$d_0 = -N \log \beta. \tag{3.25}$$

Likewise, the unit cost $\tilde{d_0}$ associated with each of the background events is given by

$$\tilde{d_0} = -\log \tilde{\beta}. \tag{3.26}$$

The unit cost of each event x_{ij} associated with a cluster k of size $n_k > 1$ equals

$$\begin{aligned} d(t_{ij}, f_{ij}; c, \theta) = &\frac{1}{2} \log 2\pi s_{ti} + \frac{1}{2s_{ti}} (t_{ij} - \bar{t}_k - \delta_{ti})^2 \\ &+ \frac{1}{2} \log 2\pi s_{fi} + \frac{1}{2s_{fi}} (f_{ij} - \bar{f}_k - \delta_{fi})^2. \end{aligned} \tag{3.27}$$

This cost depends on the choice c of clusters and on the parameters θ. Indeed, the parameters $\bar{t}_k$ and $\bar{f}_k$ are dependent on c and θ as follows:

$$\bar{t}_k = \frac{\sum_{i=1}^{N} \sum_{j=1}^{L_i} \delta[c_{ij} - k]\, w_{ti}(t_{ij} - \delta_{ti})}{\sum_{i=1}^{N} \sum_{j=1}^{L_i} \delta[c_{ij} - k]\, w_{ti}}, \tag{3.28}$$

$$\bar{f}_k = \frac{\sum_{i=1}^{N} \sum_{j=1}^{L_i} \delta[c_{ij} - k]\, w_{fi}(f_{ij} - \delta_{fi})}{\sum_{i=1}^{N} \sum_{j=1}^{L_i} \delta[c_{ij} - k]\, w_{fi}}, \tag{3.29}$$

with $w_{ti} = s_{ti}^{-1}$ and $w_{fi} = s_{fi}^{-1}$. The distance $d(t_{ij}, f_{ij})$, equation 3.27, is illustrated in Figure 5b.

Note that the second and fourth terms on the right-hand side of equation 3.27 are normalized Euclidean distances. Since the point processes $(x_i)_{1,\ldots,N}$ are defined on the time-frequency plane (see Figure 4), the (normalized) Euclidean distance is indeed a natural metric. In some applications, the point process may be defined on more general spaces, in particular, curved spaces. In such situations, one may adopt non-Euclidean distance measures. We refer to Dauwels, Vialatte et al. (2008) for an example. To simplify the notation, we define the unit cost of each event x_{ij} associated with a cluster k of size $n_k = 1$ as $d(t_{ij}, f_{ij}; c, \theta) = 0$.

We also define costs $d(s_t) = -\log p(s_t)$, $d(s_f) = -\log p(s_f)$, and $d(\theta) = d(s_t) + d(s_f)$. With those definitions of unit costs, we can rewrite equation 3.24 as

$$\begin{aligned} -\log p(x, c, \theta) = {} & d(\theta) + L d_0 + \tilde{\ell}\tilde{d}_0 \\ & + \sum_{k=1}^{L} \sum_{(i,j) \in \mathcal{I}_k} d(t_{ij}, f_{ij}; c, \theta) + \zeta. \end{aligned} \tag{3.30}$$

This expression can be written as a function of c as follows:

$$\begin{aligned} -\log p(x, c, \theta) = {} & d(\theta) + d_0 \max_{ij} c_{ij} + \tilde{d}_0 \sum_{ij} \delta[c_{ij}] \\ & + \sum_{k=1}^{\max_{ij} c_{ij}} \sum_{i=1}^{N} \sum_{j=1}^{L_i} \delta[c_{ij} - k]\, d(t_{ij}, f_{ij}; c, \theta) + \tilde{\zeta}, \end{aligned} \tag{3.31}$$

where $d(t_{ij}, f_{ij}; c, \theta)$ is given by equation 3.27. Clearly, the right-hand side of equation 3.31 depends on c in a nonlinear fashion (see equations 3.27–3.29).

4 Statistical Inference

A reasonable approach to infer (c, θ) is a maximum a posteriori (MAP) estimation,

$$(\hat{c}, \hat{\theta}) = \underset{(c,\theta)}{\operatorname{argmax}} \log p(x, c, \theta), \tag{4.1}$$

subject to equation 3.11. There is no closed-form expression for equation 4.1; therefore, we need to resort to numerical methods. A simple technique to try to solve equation 4.1 is cyclic maximization. We first choose initial values $\hat{\theta}^{(0)}$ and then perform the following updates for $\kappa \geq 1$ until convergence:

$$\hat{c}^{(\kappa)} = \underset{c}{\operatorname{argmax}} \log p(x, c, \hat{\theta}^{(\kappa-1)}), \tag{4.2}$$

$$\hat{\theta}^{(\kappa)} = \underset{\theta}{\operatorname{argmax}} \log p(x, \hat{c}^{(\kappa)}, \theta), \tag{4.3}$$

where equation 4.2 is determined subject to equation 3.11. The update, equation 4.3, of the parameters θ is straightforward and may be carried out by cyclic maximization (see appendix B for details). The update, equation 4.2, is far less straightforward; it involves an intractable optimization problem. We circumvent this issue by solving a related tractable optimization problem. In the following, we describe that problem.

The update, equation 4.2, may be expanded as

$$\hat{c}^{(\kappa)} = \underset{c}{\operatorname{argmin}} \Big(d_0 \max_{ij} c_{ij} + \tilde{d}_0 \sum_{ij} \delta[c_{ij}] + \sum_{k=1}^{\max_{ij} c_{ij}} \sum_{i=1}^{N} \sum_{j=1}^{L_i} \delta[c_{ij} - k]\, d(t_{ij}, f_{ij}; c, \hat{\theta}^{(\kappa-1)}) \Big), \tag{4.4}$$

which is also determined subject to equation 3.11.

4.1 Equivalent (Intractable) Optimization Problem. The optimization problem, equation 4.4, is hard to solve directly, and therefore we will solve a related tractable optimization problem instead. In order to formulate the latter, we introduce the following binary variables:

- b_k is equal to one iff cluster k is nonempty ($n_k > 0$ and $k = 1, 2, \ldots, L^{\text{tot}}$).
- b_{ijk} is equal to one iff the x_{ij} belongs to cluster k, that is, $c_{ij} = k$.
- e_{ij} is equal to one iff x_{ij} is a background event.

We now rewrite equation 4.4 using that notation, which will allow us to simplify the combinatorial problem in section 4.2.

The binary variables b are related through the constraints

$$b_k = \min\left(1, \sum_{i=1}^{N}\sum_{j=1}^{L_i} b_{ijk}\right), \quad \forall k. \tag{4.5}$$

These nonlinear inequality constraints are equivalent to the linear constraints,

$$b_{ijk} \le b_k, \quad \forall i, j, k, \quad \text{and} \quad \sum_{i=1}^{N}\sum_{j=1}^{L_i} b_{ijk} \ge b_k, \quad \forall k. \tag{4.6}$$

The constraints 3.11 correspond to

$$\sum_{j=1}^{L_i} b_{ijk} \le 1, \quad \forall i, k. \tag{4.7}$$

Moreover, an event is either a background event or belongs to a cluster, which can be encoded by the constraints

$$\sum_{k}^{L} b_{ijk} + e_{ij} = 1, \quad \forall i, j, \tag{4.8}$$

In this representation, we can rewrite equation 4.4 as

$$\begin{aligned}\left(\hat{b}^{(\kappa)}, \hat{e}^{(\kappa)}\right) = \underset{b,e}{\operatorname{argmin}} \Bigg(& d_0 \sum_{k=1}^{L^{\mathrm{tot}}} b_k + \tilde{d}_0 \sum_{i=1}^{N}\sum_{j=1}^{L_i} e_{ij} \\ & + \sum_{k=1}^{L^{\mathrm{tot}}}\sum_{i=1}^{N}\sum_{j=1}^{L_i} b_{ijk}\, d\left(t_{ij}, f_{ij}; b, \hat{\theta}^{(\kappa-1)}\right)\Bigg),\end{aligned} \tag{4.9}$$

subject to equations 4.6 to 4.8. As we pointed out earlier, the number of clusters is at most L^{tot}, the total number of events.

If x_{ij} is associated with a cluster k of size $n_k > 1$, and hence $\sum_{i=1}^{N}\sum_{j=1}^{L_i} b_{ijk} > 1$, the expression $d(t_{ij}, f_{ij}; b, \hat{\theta}^{(\kappa-1)})$ in equation 4.9 is given by

equation 3.27 (see Figure 5b), with $\theta = \hat{\theta}^{(\kappa-1)}$ and

$$\bar{t}_k = \frac{\sum_{i=1}^{N} \sum_{j=1}^{L_i} b_{ijk}\, \hat{w}_{ti}^{(\kappa-1)} (t_{ij} - \hat{\delta}_{ti}^{(\kappa-1)})}{\sum_{i=1}^{N} \sum_{j=1}^{L_i} b_{ijk}\, \hat{w}_{ti}^{(\kappa-1)}} \tag{4.10}$$

$$\bar{f}_k = \frac{\sum_{i=1}^{N} \sum_{j=1}^{L_i} b_{ijk}\, \hat{w}_{fi}^{(\kappa-1)} (f_{ij} - \hat{\delta}_{fi}^{(\kappa-1)})}{\sum_{i=1}^{N} \sum_{j=1}^{L_i} b_{ijk}\, \hat{w}_{fi}^{(\kappa-1)}}, \tag{4.11}$$

where $\hat{w}_{ti}^{(\kappa-1)} = (\hat{s}_{ti}^{(\kappa-1)})^{-1}$ and $\hat{w}_{fi}^{(\kappa-1)} = (\hat{s}_{fi}^{(\kappa-1)})^{-1}$; otherwise $d(t_{ij}, f_{ij}; b, \hat{\theta}^{(\kappa-1)}) = 0$.

By exponentiating the objective function in equation 4.9, and adding the priors in θ, we obtain the statistical model:

$$p\big(x, b, e, \hat{\theta}^{(\kappa-1)}\big) \propto p\big(\hat{s}_t^{(\kappa-1)}\big) p\big(\hat{s}_f^{(\kappa-1)}\big) \prod_{k=1}^{L^{\text{tot}}} \big(\beta^N\big)^{b_k} \prod_{i=1}^{N} \prod_{j=1}^{L_i} \tilde{\beta}^{e_{ij}}$$

$$\cdot \prod_{k=1}^{L^{\text{tot}}} \prod_{i=1}^{N} \prod_{j=1}^{L_i} \big(\mathcal{N}(t_{ij} - \bar{t}_k; \delta_{ti}, s_{ti})\, \mathcal{N}(f_{ij} - \bar{f}_k; \delta_{fi}, s_{fi})\big)^{b_{ijk}}, \tag{4.12}$$

which is equivalent to equation 3.23. Likewise, the constrained combinatorial optimization problem, equations 4.6 to 4.9, is equivalent to equation 4.4. It is a nonlinear combinatorial optimization problem, since the objective function (the right-hand side of equation 4.9) is nonlinear in b. Since the problem is intractable, we simplify it. We linearize the objective function by using an exemplar representation. The resulting linear combinatorial optimization problem (the integer linear program, ILP) can then be solved exactly by integer linear programming. In other words, we will approximate the original nonlinear and intractable integer program, equations 4.6 to 4.9 (which is hard to solve directly), into a linear and tractable integer program (which is much easier to solve).

4.2 Related (Tractable) Optimization Problem. Ideally, we wish to find the cluster centers $(\bar{t}_k, \bar{f}_k)$, equations 4.10 and 4.11, that minimize the combined total cost $d(t_{ij}, f_{ij})$, equation 3.27, of all events in the cluster. That is an intractable problem, and we simplify it as follows. Rather than searching through all possible cluster centers, we consider only events x_{ij} as potential cluster centers. In other words, we consider a restricted subset of potential centers. More specifically, we approximate the cluster center $(\bar{t}_k, \bar{f}_k)$ by the event x_{ij} of the same cluster that lies the closest to the center, after eliminating the offset $(\delta_{ti}, \delta_{fi})$ (see Figure 5c). The events x_{ij} that serve as cluster

centers are referred to as exemplars. This approach is inspired by other exemplar-based clustering algorithms, including affinity propagation (Frey & Dueck, 2007) and recent extensions (Lashkari & Golland, 2008; Givoni & Frey, 2009).

As a result, the nonlinear cost $d(t_{ij}, f_{ij})$, equation 3.27, is approximated by a cost that is independent of b; the nonlinear objective function (the right-hand side of equation 4.9) becomes linear in b, and hence the nonlinear combinatorial optimization problem, equation 4.9, is approximated by an integer linear program. We now derive this integer linear program. Similarly to the variables b_k and b_{ijk}, we introduce the following binary variables:

- b_{ij} is equal to one iff x_{ij} is an exemplar.
- $b_{iji'j'}$ is equal to one iff x_{ij} is associated with exemplar $x_{i'j'}$.

In this formulation, we approximate the intractable optimization problem, equations 4.6 to 4.9, by the following integer linear program in b:

$$\begin{aligned}\left(\hat{b}^{(\kappa)}, \hat{e}^{(\kappa)}\right) = \underset{b,e}{\operatorname{argmin}} \Bigg(& d_0 \sum_{i=1}^{N} \sum_{j=1}^{L_i} b_{ij} + \tilde{d}_0 \sum_{i=1}^{N} \sum_{j=1}^{L_i} e_{ij} \\ & + \sum_{i,i'=1}^{N} \sum_{j=1}^{L_i} \sum_{j'=1}^{L_{i'}} b_{iji'j'}\, d\left(t_{ij}, f_{ij}, t_{i'j'}, f_{i'j'}; \hat{\theta}^{(\kappa-1)}\right) \Bigg),\end{aligned} \tag{4.13}$$

subject to

$$\sum_{i'j'} b_{iji'j'} + b_{ij} + e_{ij} = 1, \quad \forall i, j, \tag{4.14}$$

$$\sum_{j=1}^{L_i} b_{iji'j'} \leq b_{i'j'}, \quad \forall i, i' \neq i, j', \tag{4.15}$$

$$b_{ijij'} = 0, \quad \forall i, j, j', \tag{4.16}$$

where

$$\begin{aligned} & d(t_{ij}, f_{ij}, t_{i'j'}, f_{i'j'}; \hat{\theta}^{(\kappa-1)}) \\ & = \frac{1}{2} \log 2\pi \hat{s}_{ti}^{(\kappa-1)} + \frac{1}{2\hat{s}_{ti}^{(\kappa-1)}} \left(t_{ij} - t_{i'j'} - \hat{\delta}_{ti}^{(\kappa-1)}\right)^2 \\ & \quad + \frac{1}{2} \log 2\pi \hat{s}_{fi}^{(\kappa-1)} + \frac{1}{2\hat{s}_{fi}^{(\kappa-1)}} \left(f_{ij} - f_{i'j'} - \hat{\delta}_{fi}^{(\kappa-1)}\right)^2. \end{aligned} \tag{4.17}$$

By exponentiating the objective function in equation 4.13, and adding the priors in θ, we obtain the statistical model:

$$p\big(x, b, e, \hat{\theta}^{(\kappa-1)}\big) \propto p(\hat{s}_t^{(\kappa-1)}) p(\hat{s}_f^{(\kappa-1)}) \prod_{i=1}^{N} \prod_{j=1}^{L_i} \big(\beta^N\big)^{b_{ij}} \tilde{\beta}^{e_{ij}} \cdot \prod_{i,i'=1}^{N} \prod_{j=1}^{L_i} \prod_{j'=1}^{L_{i'}}$$

$$\times \big(\mathcal{N}\big(t_{ij} - t_{i'j'}; \hat{\delta}_{ti}^{(\kappa-1)}, \hat{s}_{ti}^{(\kappa-1)}\big) \mathcal{N}\big(f_{ij} - f_{i'j'}; \hat{\delta}_{fi}^{(\kappa-1)}, \hat{s}_{fi}^{(\kappa-1)}\big)\big)^{b_{iji'j'}}. \quad (4.18)$$

The objective function equation 4.13, is a linear approximation of the nonlinear objective function, equation 4.4, and similarly, the statistical model, equation 4.18, is an approximation of $p(x, c, \hat{\theta}^{(\kappa-1)})$, equation 3.23. The resulting linear integer problem, equations 4.13 to 4.16, is much easier to solve than the nonlinear integer problem, equations 4.6–4.9. Note that both problems lead to similar results, since exemplars are often close to the cluster center (see Figure 5c).

The sum $\sum_{ij} b_{ij}$ in equation 4.13 is equal to the number of exemplars; therefore, the first term assigns a cost d_0 to each exemplar. Likewise, the second term assigns a cost $\tilde{d}_0$ to each background event. The third term associates the cost 4.17 to each event x_{ij}, based on its associated exemplar $x_{i'j'}$. This cost is independent of b, and consequently the objective function, equation 4.13, is linear in b.

The constraints, equation 4.14, ensure that each event is either an exemplar, is associated with one exemplar (and not more than one exemplar), or is a background event (insertion). The constraints, equation 4.15, encode the fact that an event x_{ij} can be associated to an exemplar $x_{i'j'}$ ($b_{iji'j'} = 1$) only iff the latter is indeed an exemplar ($b_{i'j'} = 1$); they also ensure that at most one event x_{ij} from x_i can be associated with an exemplar $x_{i'j'}$. Finally, the constraints 4.16 ensure that an event x_{ij} cannot be associated with an exemplar from the same point process x_i. Without those constraints, multiple events from the same point process x_i may belong to the same cluster, which is not allowed.

The combinatorial optimization problem, equations 4.13 to 4.16, is an integer linear program in b and e, since the objective function, equation 4.13, and constraints, equations 4.14 to 4.16, are linear in the variables b and e. More specifically, it is a binary linear program, since all variables are binary. Instead of solving the intractable problem, equation 4.4, or, equivalently, equations 4.6 to 4.9, we solve the tractable problem, equations 4.13 to 4.16, in particular, by means of off-the-shelf integer programming software.

As an alternative, we have also implemented the max-product algorithm (and various refinements) to solve equations 4.13 to 4.16, as we did for bivariate SES (Dauwels et al., 2009a, 2009b). Unfortunately, that approach leads to poor results for N-variate SES. In particular, it does not always converge, and sometimes it yields solutions that violate the constraints 4.14

to 4.16. Those issues might be due to the fact that N-wise alignment is significantly more complex than pairwise alignment.

Note that it is straightforward to determine estimates $\hat{\rho}$, $(\hat{p}_j)_{j=1}^N$, and $\hat{\chi}$ from $\hat{b}$ and $\hat{e}$. Also, an estimate $\hat{c}$ can easily be computed from $\hat{b}$ and $\hat{e}$ as follows. We number all exemplars from 1 to L, in arbitrary order. We then set $\hat{c}_{ij} = k$ if x_{ij} is the kth exemplar or if it is associated with the kth exemplar. Likewise we set $\hat{c}_{ij} = 0$ if x_{ij} is a background event ($\hat{e}_{ij} = 1$). The resulting estimate $\hat{c}$ is an approximation of equation 3.4. With this estimate of $\hat{c}$, we can eventually refine the estimate θ, following rule 4.3.

The resulting SES inference algorithm is summarized in Table 2.

5 Extensions

So far, we have developed N-variate SES for the particular example of bump models in the time-frequency domain. The statistical model, equation 3.23, and, equivalently, the cost function, equation 3.31, may easily be generalized, and it may be applied to different kinds of point processes. One simply needs to define the cost functions d in equation 3.31 in a suitable manner. We briefly outline several potential extensions and alternative applications.

- As we pointed out in Dauwels et al. (2009b), we normalized the parameters (δ_t, s_t) and (δ_f, s_f) by the width and height of the bumps, respectively, in order to take the size of the bumps into account. Such normalization factors can easily be incorporated in cost function 3.31. The unit cost $d(t_{ij}, f_{ij}; c, \theta)$ of an event x_{ij} is then defined as

$$d(t_{ij}, f_{ij}; c, \theta) = \frac{1}{2}\log 2\pi\bar{s}_{ti} + \frac{1}{2\bar{s}_{ti}}(t_{ij} - \bar{t}_k - \bar{\delta}_{ti})^2 + \frac{1}{2}\log 2\pi\bar{s}_{fi} + \frac{1}{2\bar{s}_{fi}}(f_{ij} - \bar{f}_k - \bar{\delta}_{fi})^2, \tag{5.1}$$

  with $\bar{\delta}_{ti} = \delta_{ti}\,\Delta t_k$, $\bar{\delta}_{fi} = \delta_{fi}\,\Delta f_k$, $\bar{s}_{ti} = s_{ti}\,\Delta t_k^2$, and $\bar{s}_{fi} = s_{fi}\,\Delta f_k^2$, where Δt_k and Δf_k are the average width and height, respectively, of the bumps x_{ij} in cluster k.
- As we outlined in Dauwels et al. (2009b, sect. 6), one can easily incorporate differences in amplitude, width, and height between the bumps of the different point processes. Moreover, the bumps may be oblique; they are not necessarily parallel to the time and frequency axes.
- Until now we have considered bump models in the time-frequency domain. However, the statistical model, equation 3.23, and, equivalently, the cost function, equation 3.30, are readily extendable to point processes in other Euclidean spaces (e.g., three-dimensional spatial point processes or one-dimensional point processes in time domain).

Input
One-dimensional or multidimensional point processes $(x_i)_{i=1}^N$ and parameters β, $\tilde{\beta}$, ν_t, ν_f, s_{t0}, s_{f0}, $(\hat{\delta}_{ti}^{(0)})_{i=1}^N$, $(\hat{\delta}_{fi}^{(0)})_{i=1}^N$, $(\hat{s}_{ti}^{(0)})_{i=1}^N$, $(\hat{s}_{fi}^{(0)})_{i=1}^N$.

Algorithm
Iterate the following two steps until convergence or the available time has elapsed:

1. Update the clustering $(\hat{b}, \hat{e})$ (and equivalently $\hat{c}$) by ILP:

$$(\hat{b}^{(\kappa)}, \hat{e}^{(\kappa)}) = \underset{b,e}{\operatorname{argmin}} \Bigg(d_0 \sum_{i=1}^{N} \sum_{j=1}^{L_i} b_{ij} + \tilde{d}_0 \sum_{i=1}^{N} \sum_{j=1}^{L_i} e_{ij} + \sum_{i,i'=1}^{N} \sum_{j=1}^{L_i} \sum_{j'=1}^{L_{i'}} b_{iji'j'} \, d(t_{ij}, f_{ij}, t_{i'j'}, f_{i'j'}; \hat{\theta}^{(\kappa-1)}) \Bigg),$$

   subject to equations 4.14 to 4.16.

2. Update the SES parameters:

   Solve the equations:

$$\hat{\delta}_{ti}^{(\kappa)} = \frac{1}{L_i} \sum_{j=1}^{L_i} \left(t_{ij} - \bar{t}_{\hat{c}_{ij}^{(\kappa)}} \right)$$

$$\hat{\delta}_{fi}^{(\kappa)} = \frac{1}{L_i} \sum_{j=1}^{L_i} \left(f_{ij} - \bar{f}_{\hat{c}_{ij}^{(\kappa)}} \right)$$

$$\hat{s}_{ti}^{(\kappa)} = \frac{\nu_t s_{t0} + L_i \, \hat{s}_{ti,\text{sample}}^{(\kappa)}}{\nu_t + L_i + 2}$$

$$\hat{s}_{fi}^{(\kappa)} = \frac{\nu_f s_{f0} + L_i \, \hat{s}_{fi,\text{sample}}^{(\kappa)}}{\nu_f + L_i + 2},$$

   with

$$\bar{t}_k = \frac{\sum_{(i,j) \in \hat{\mathcal{I}}_k^{(\kappa)}} \hat{w}_{ti}^{(\kappa)} (t_{ij} - \hat{\delta}_{ti}^{(\kappa)})}{\sum_{(i,j) \in \hat{\mathcal{I}}_k^{(\kappa)}} \hat{w}_{ti}^{(\kappa)}} \qquad \bar{f}_k = \frac{\sum_{(i,j) \in \hat{\mathcal{I}}_k^{(\kappa)}} \hat{w}_{fi}^{(\kappa)} (f_{ij} - \hat{\delta}_{ti}^{(\kappa)})}{\sum_{(i,j) \in \hat{\mathcal{I}}_k^{(\kappa)}} \hat{w}_{fi}^{(\kappa)}}.$$

Output
Clustering $(\hat{b}, \hat{e})$ (and equivalently $\hat{c}$) and SES parameters $\hat{\rho}$, $\hat{\chi}$, $(\hat{p}_j)_{j=1}^N$, $(\hat{\delta}_{ti})_{i=1}^N$, $(\hat{\delta}_{fi})_{i=1}^N$, $(\hat{s}_{ti})_{i=1}^N$, $(\hat{s}_{fi})_{i=1}^N$.

Table 2: Inference Algorithm for N-Variate SES.

We will consider an example of the latter in section 7. The unit cost $d(t_{ij}; c, \theta)$ of an event x_{ij} may then defined as

$$d(t_{ij}; c, \theta) = \frac{1}{2} \log 2\pi s_{ti} + \frac{1}{2s_{ti}} (t_{ij} - \bar{t}_k - \delta_{ti})^2, \tag{5.2}$$

where we did not take the widths of the events into account. If the latter need to be taken into account, we may normalize the parameters (δ_{ti}, s_{ti}) as in equation 5.1.

- In some applications, the point processes may be defined on curved manifolds, and non-Euclidean distances are then more natural. For instance, the point processes may be defined on planar closed curves. We refer to Dauwels, Tsukada et al. (2008) for an example. The unit cost $d(t_{ij}; c, \theta)$ of an event x_{ij} may then be defined by

$$d(t_{ij}; c, \theta) = \frac{1}{2} \log 2\pi s_{ti} + \frac{1}{2s_{ti}} \big(g(t_{ij}, \bar{t}_k) - \delta_{ti}\big)^2, \tag{5.3}$$

where $\bar{t}_k$ is the center of cluster k, defined as

$$\bar{t}_k = \text{argmin}_t \sum_{(i,j) \in \mathcal{I}_k} \frac{1}{s_{ti}} \big(g(t_{ij}, t) - \delta_{ti}\big)^2, \tag{5.4}$$

where g is an arbitrary function, potentially nonlinear; for $g(x, y) = x - y$, we recover equation 5.2.

6 Analysis of Synthetic Data

We investigate the robustness and reliability of N-variate SES by means of synthetic data. We consider one-dimensional and two-dimensional point processes, as in Parts I (Dauwels et al., 2009a) and II (Dauwels et al., 2009b), respectively. We discuss the results for one-dimensional and two-dimensional point processes in sections 6.1 and 6.2, respectively.

6.1 One-Dimensional Point Processes. We randomly generated 1000 sets of $N = 5$ one-dimensional point processes according to the generative process outlined in section 3.

We tested several values of the parameters p_d, δ_{ti}, and s_{ti} (σ_{ti}), for $i = 1, 2, \ldots, 5$. In particular, we tested the values $p_d = 0, 0.1, \ldots, 0.4$, and $\sigma_{ti} =$ 10 ms, 30 ms, and 50 ms (for $i = 1, 2, \ldots, 5$), $t_{\text{min}} = 0$ ms, and $t_{\text{max}} = \ell_0 \cdot 100$ ms. The length ℓ was chosen as $\ell = \ell_0/(1 - p_d)$, where we tested the values $\ell_0 = 40, 100$. With this choice, the expected length of the point processes is ℓ_0, independent of p_d. In one set of experiments, we set $\delta_{ti} = 0$, for $i = 1, 2, \ldots, 5$. In a second set, the offsets δ_{ti} are drawn uniformly within $[-50 \text{ ms}, 50 \text{ ms}]$. In each case, we did not insert events (see step 4).

We used the initial values $\hat{\delta}_{ti}^{(0)} = 0$ ms, and $\hat{s}_{ti}^{(0)} = (20 \text{ ms})^2, (30 \text{ ms})^2$, for $i = 1, 2, \ldots, 5$. The parameter β was identical for all parameter settings:

$\beta = 0.04$. It was optimized to yield the best overall results. We used an uninformative prior for δ_{ti} and s_{ti}: $p(\delta_{ti}) = p(s_{ti}) = 1$, for $i = 1, 2, \ldots, 5$. One could test various initial values of $\hat{\delta}_{ti}$, for $i = 1, 2, \ldots, 5$. However, the number of initial conditions grows exponentially with N, and therefore it is not really practical to test multiple values for each $\hat{\delta}_{ti}^{(0)}$. For example, if we test three values for each $\hat{\delta}_{ti}^{(0)}$, we need to test a total of $3^5 = 243$ initial values $\hat{\delta}_{ti}^{(0)}$. Alternatively, one may use a small, random subset of initial values; for conciseness, we do not consider that approach here.

We set $\tilde{\beta} = 10^{-20}$, as in all our simulations in this letter. For the synthetic data, no background events were inferred (i.e., $\chi = 0$ for all parameter settings).

In order to assess the SES measures $S = s_t, \rho$, we compute for each above-mentioned parameter setting the expectation $\mathrm{E}[S]$ and normalized standard deviation $\overline{\sigma}[S] = \sigma[S]/\mathrm{E}[S]$. Those statistics are computed by averaging over 1000 sets of five point processes, randomly generated according to the generative process outlined in section 3.

The results are summarized in Figure 6. From this figure, we can make the following observations:

- The estimates of s_t and p_d are slightly biased, especially for small ℓ_0—$\ell_0 = 40$, $s_t \geq (30\ \mathrm{ms})^2$, and $p_d > 0.2$. However, the bias is significantly smaller than for bivariate SES (see Dauwels et al., 2009a).
- The estimates of s_t only weakly depend on p_d, and vice versa.
- The estimates of s_t and p_d only weakly depend on δ_{ti} (curved versus solid lines); they are robust to lags δ_t. Note that one could reduce this dependency further by testing various initial values $\hat{\delta}_{ti}^{(0)}$. However, the number of initial conditions grows exponentially with N, as we mentioned earlier; therefore, this approach is not really practical.
- The estimates of s_t and p_d are less biased for larger ℓ_0.

We have also observed from our experiments (not shown here):

- The estimates of δ_t are unbiased for all considered values of δ_t, s_t, and p_d.
- The normalized standard deviation of the estimates of δ_t, s_t, and p_d grows with s_t and p_d, but it remains below 30%. Those estimates are therefore reliable.
- The normalized standard deviation of the SES parameters decreases as the length ℓ_0 increases, as expected.

6.2 Two-Dimensional Point Processes. Similarly as in the one-dimensional case, we randomly generated 1000 sets of $N = 5$ two-dimensional point processes according to the generative process outlined in section 3.

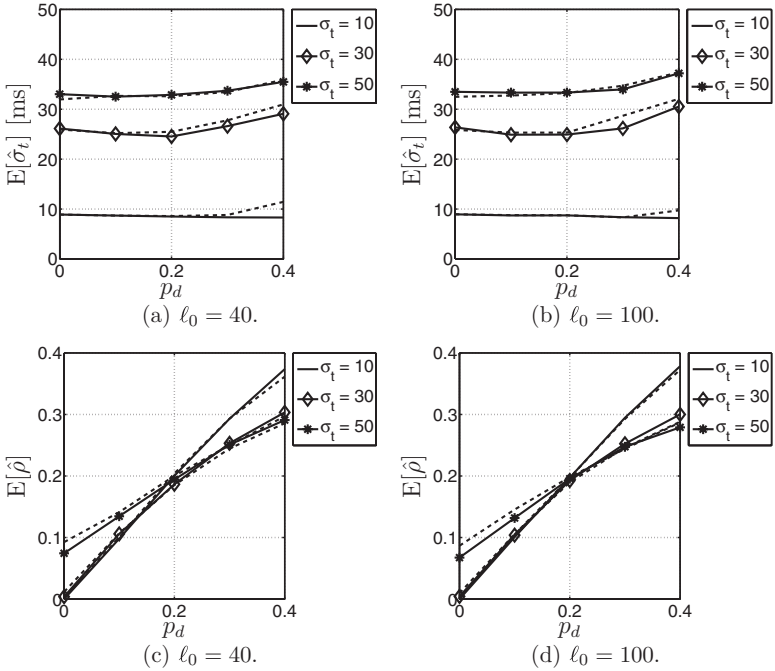

Figure 6: Results for N-variate stochastic event synchrony for one-dimensional point processes. The figure shows the expected value $\mathrm{E}[\hat{\sigma}_t]$ and $\mathrm{E}[\hat{\rho}]$ for the parameter settings $\ell_0 = 40, 100$, $\sigma_t = 10, 30, 50$ ms, and $p_d = 0, 0.1, \ldots, 0.4$. The solid lines are for zero delays δ_{ti}, whereas the dotted lines are for offsets δ_{ti} drawn uniformly within $[-50 \text{ ms}, 50 \text{ ms}]$.

We considered several values of the parameters p_d, δ_{ti}, s_{ti} (σ_{ti}), δ_{fi}, and s_{fi} (σ_{fi}), for $i = 1, 2, \ldots, 5$. In particular, we tested the values $p_d = 0, 0.1, \ldots, 0.4$, and $\sigma_{ti} = 10$ ms, 30 ms, and 50 ms, $\sigma_{fi} = 1$ Hz, 2.5 Hz, 5 Hz (for $i = 1, 2, \ldots, 5$), $t_{\min} = 0$ ms, and $t_{\max} = \ell_0 \cdot 100$ ms, $f_{\min} = 0$ Hz, and $f_{\max} = \ell_0 \cdot 1$ Hz. The length ℓ was chosen as $\ell = \ell_0/(1 - p_d)$, where we tested the values $\ell_0 = 40, 100$. With this choice, the expected length of the point processes is ℓ_0, independent of p_d. In one set of experiments, we set $\delta_{ti} = 0 = \delta_{fi}$, for $i = 1, 2, \ldots, 5$. In a second set, the offsets δ_{ti} and δ_{fi} are drawn uniformly within $[-50 \text{ ms}, 50 \text{ ms}]$ and $[-5 \text{ Hz}, 5 \text{ Hz}]$, respectively. In each case, we did not insert events (see step 4).

We used the initial values $\hat{\delta}_{ti}^{(0)} = 0$ ms, $\hat{\delta}_{fi}^{(0)} = 0$ Hz, $\hat{s}_{ti}^{(0)} = (20 \text{ ms})^2, (30 \text{ ms})^2$, and $\hat{s}_{fi}^{(0)} = (2 \text{ Hz})^2$, for $i = 1, 2, \ldots, 5$. The parameter β was identical for all parameter settings: $\beta = 0.01$. It was optimized to yield the best overall

results. We used an uninformative prior for δ_{ti}, δ_{fi}, s_{ti}, and s_{fi}: $p(\delta_{ti}) = p(s_{ti}) = p(\delta_{fi}) = p(s_{fi}) = 1$.

The results are summarized in Figures 7 to 9. Overall, they are quite similar to the ones for one-dimensional point processes (see Figure 6). We observe the following:

- The estimates of s_t and p_d are slightly biased. However, the bias is significantly smaller than in the one-dimensional case, as for bivariate SES (see Figure 4 and section 7 in Dauwels et al., 2009b).
- The bias increases with s_f, which is in agreement with our expectations: the more frequency jitter there is, the more likely that some events are reversed in frequency, and hence are aligned incorrectly. The bias is about the same as for bivariate SES (see Dauwels et al., 2009b).
- The estimates of s_t only weakly depend on p_d, and vice versa.
- The estimates of s_t and p_d are robust to lags δ_t and frequency offsets δ_f, since the latter can be estimated reliably.
- The estimates of s_t and p_d are less biased for larger ℓ_0.

We have also observed from our experiments (not shown here):

- The estimates of δ_t and δ_f are unbiased for all considered values of δ_t, δ_f, s_t, s_f, and p_d.
- The normalized standard deviation of the estimates of δ_t, s_t, and p_d grows with s_t and p_d, but it remains below 30%. Those estimates are therefore reliable.
- The normalized standard deviation of the SES parameters decreases as the length ℓ_0 increases, as expected.

In summary, by means of the N-variate SES inference method, one may reliably and robustly determine the timing dispersion s_t and event reliability ρ of a set of N (one-dimensional or multidimensional) point processes. As we also observed in Dauwels et al. (2009a, 2009b) for bivariate SES, the timing dispersion and the number of event deletions are slightly underestimated due to the ambiguity inherent in event synchrony. However, this bias is smaller for N-variate SES than for bivariate SES, especially for one-dimensional point processes.

7 Application: Firing Reliablity of a Neuron

We consider here an application of SES that we also investigated in Dauwels et al. (2009a): we use SES to quantify the firing reliability of neurons. We again consider the Morris-Lecar neuron model (Morris & Lecar, 1981), which exhibits properties of type I and II neurons (Gutkin & Ermentrout, 1998; Tsumoto, Kitajima, Yoshinaga, Aihara, & Kawakami, 2007; Tateno & Pakdaman, 2004). The spiking behavior differs in both neuron types, as

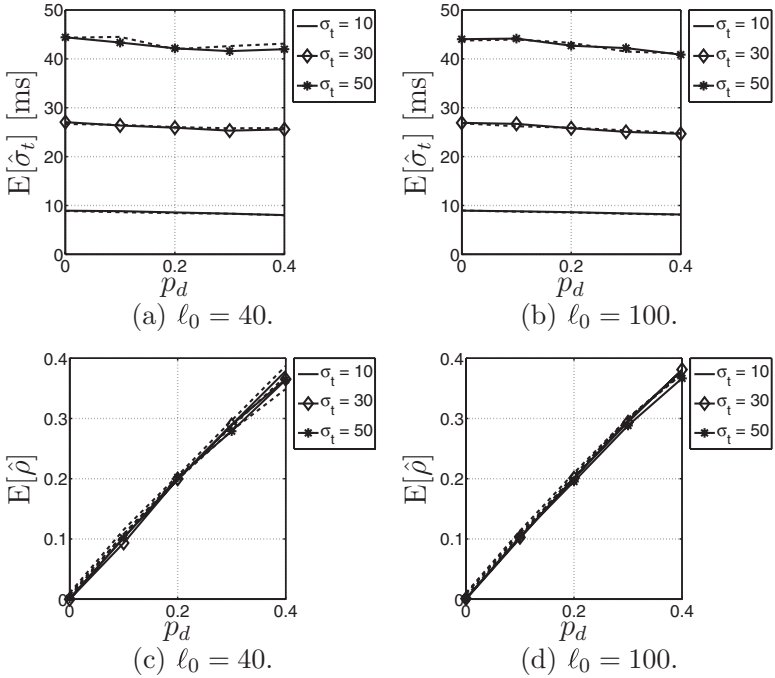

Figure 7: Results for synthetic data. The figure shows the expected value $\mathrm{E}[\hat{\sigma}_t]$ and $\mathrm{E}[\hat{\rho}]$ and the normalized standard deviation $\bar{\sigma}[\hat{\sigma}_t]$ and $\bar{\sigma}[\hat{\rho}]$ for the parameter settings $\ell_0 = 40, 100$, $\sigma_t = 10, 30, 50$ ms, $p_d = 0, 0.1, \ldots, 0.4$, and $\sigma_f = 1$ Hz. The solid lines are for zero delays δ_{ti}, whereas the dotted lines are for offsets δ_{ti} and δ_{fi}, drawn uniformly within $[-50$ ms, 50 ms] and $[-5$ Hz, 5 Hz], respectively. The curves for zero and random delays are practically coinciding.

illustrated in Figure 10. In type II neurons, the timing jitter is small, but spikes tend to drop out. In type I neurons, fewer spikes drop out, but the dispersion of spike times is larger. In other words, type II neurons prefer to stay coherent or to be silent, and, type I neurons follow the middle course between those two extremes (Robinson, 2003).

In Dauwels et al. (2009a) we applied bivariate SES to the data of Figure 10. Here we apply N-variate SES to the same data set. (We refer to Dauwels et al., 2009a, for more details on that data set.) In particular, we apply N-variate SES to the 50 trials simultaneously.

As an illustration, we show results of N-variate SES in Figure 11. Each cluster is indicated by a different combination of shading and marker type (e.g., star, circle); background events are marked by hexagons.

We choose the parameters in the N-variate SES algorithm as follows. We set $\hat{\delta}_t^{(0)} = 0$, and $\hat{s}_t^{(0)} = (3 \text{ ms})^2$, $(5 \text{ ms})^2$, $(7 \text{ ms})^2$ and $(9 \text{ ms})^2$. Each

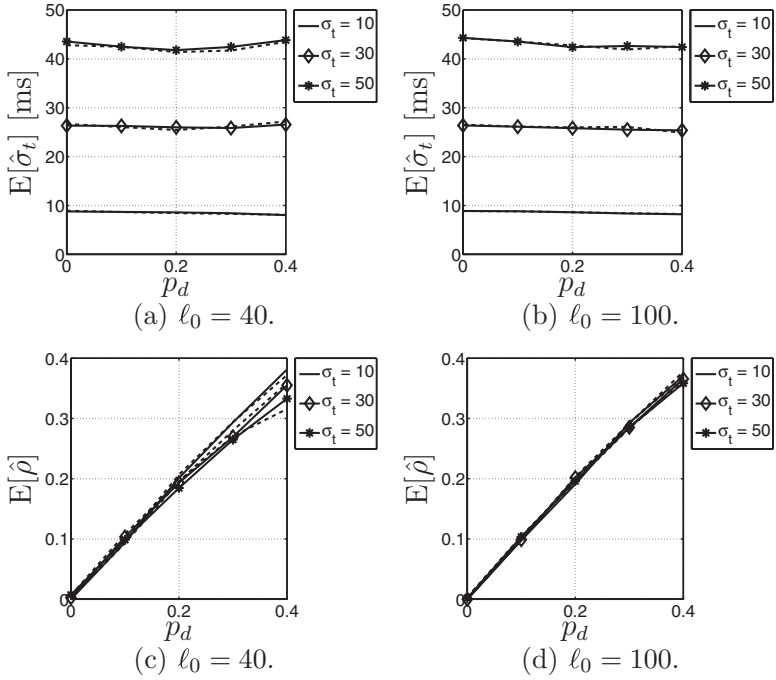

Figure 8: Results for synthetic data. The figure shows the expected value $\mathrm{E}[\hat{\sigma}_t]$ and $\mathrm{E}[\hat{\rho}]$ and the normalized standard deviation $\bar{\sigma}[\hat{\sigma}_t]$ and $\bar{\sigma}[\hat{\rho}]$ for the same parameter settings as in Figure 7, but now with $\sigma_f = 2.5$ Hz. Again, the curves for zero and random delays are practically coinciding.

initialization of $(\hat{\delta}_t^{(0)}, \hat{s}_t^{(0)})$ may lead to a different solution $(\hat{c}, \hat{\delta}_t, \hat{s}_t)$; we choose the most probable solution—the one that has the largest value $p(x, \hat{c}, \hat{\delta}_t, \hat{s}_t)$ (see equation 3.23). We set $\tilde{\beta} = 10^{-10}$. Larger values of $\tilde{\beta}$ lead to a prohibitively large number of background events, whereas smaller values yield no background events at all.

We computed the SES parameters for different values of β. Figure 12 shows how s_t (σ_t), ρ, and χ (fraction of background events) depend on β for both neuron types. From those figures, it becomes immediately clear that the parameters s_t (σ_t) and ρ hardly depend on β. For values of $\beta < 10^{-4}$, some of the events from the type II neuron are considered as background events, which is obviously incorrect (see Figure 11b). Therefore, only values $\beta > 10^{-4}$ should be considered.

The parameter ρ is significantly smaller in type I than in type II neurons; in contrast, s_t is vastly larger. This agrees with our intuition. Since in type II neurons, spikes tend to drop out, ρ should be larger. On the other hand,

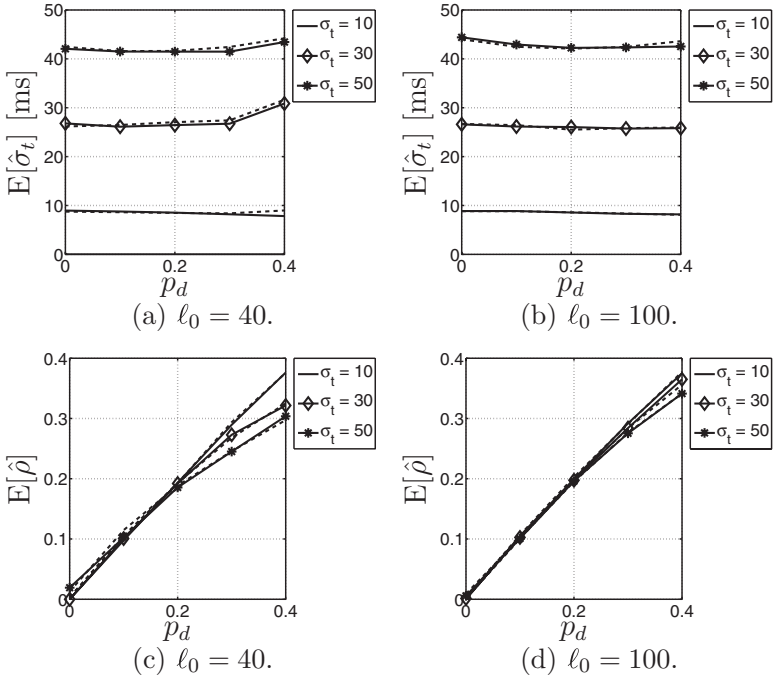

Figure 9: Results for synthetic data. The figure shows the expected value $\mathrm{E}[\hat{\sigma}_t]$ and $\mathrm{E}[\hat{\rho}]$ and the normalized standard deviation $\bar{\sigma}[\hat{\sigma}_t]$ and $\bar{\sigma}[\hat{\rho}]$ for the same parameter settings as in Figure 7, but now with $\sigma_f = 5$ Hz. Again, the curves for zero and random delays are practically coinciding.

since the timing dispersion of the spikes in type I is larger, we expect s_t to be larger in those neurons. We made the same observations in Dauwels et al. (2009a).

Table 3 compares the numerical results for bivariate and N-variate SES. As we pointed out earlier, bivariate SES defines the variance of the perturbations in the generative process as $s_t/2$ (instead of s_t), so that the variance between the two observed sequences x_1 and x_2 is given by s_t. In Table 3, the standard deviations ($\sigma_t = \sqrt{s_t}$) in the generative process are reported for both bivariate and N-variate SES; the values in Dauwels et al. (2009a) differ by a factor $\sqrt{2}$, since there the standard deviation between the observed sequences is reported.

In Dauwels et al. (2009a) we assessed the reliability of the bivariate SES estimates by means of bootstrapping (Efron & Tibshirani, 1993). We follow a similar procedure here for the N-variate SES estimates. In particular, for both types of neurons, we generated 1000 sets of 50 spike trains; we followed the generative process of Figure 4, with the N-variate SES parameters of the

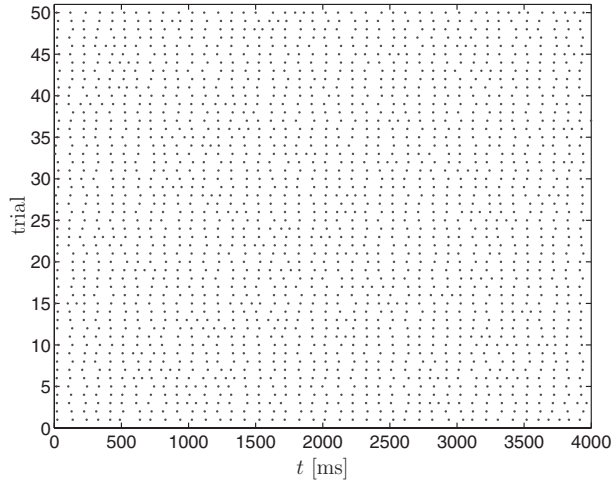

(a) Spike trains from type I neuron.

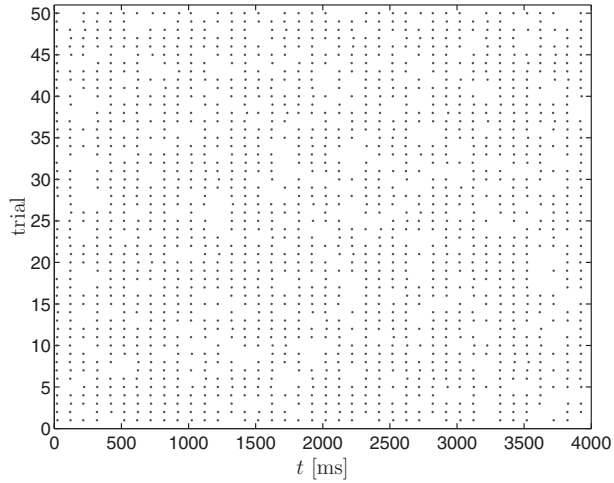

(b) Spike trains from type II neuron.

Figure 10: Raster plots of spike trains from type I (top) and type II (bottom) neurons. In each case, 50 spike trains are shown.

actual spike trains, that is, $(\rho, \sigma_t, \chi) = (10.6, 0.0025, 0.035)$ and $(\rho, \sigma_t, \chi) = (2.8, 0.18, 0.0)$ for type I and II neurons respectively. Next we applied N-variate SES to the resulting 1000 sets of 50 spike trains. The expected value and normalized standard deviation $\bar{\sigma}$ of those estimates are reported in Table 3. We can observe that the expected value corresponds well with the

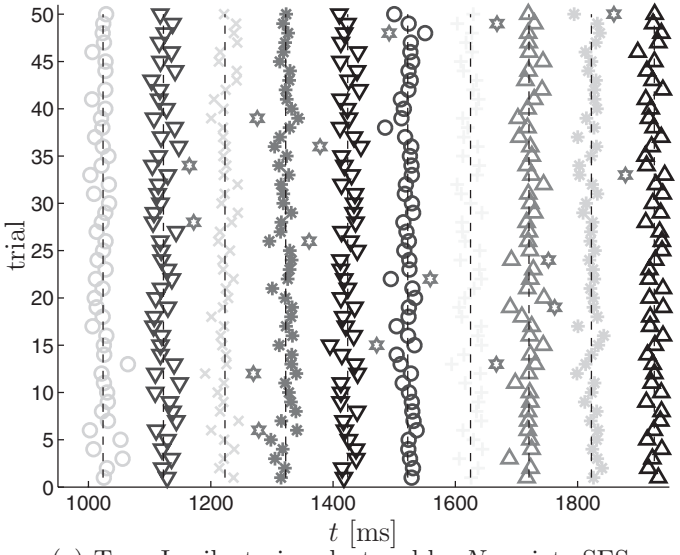

(a) Type I spike trains clustered by N-variate SES.

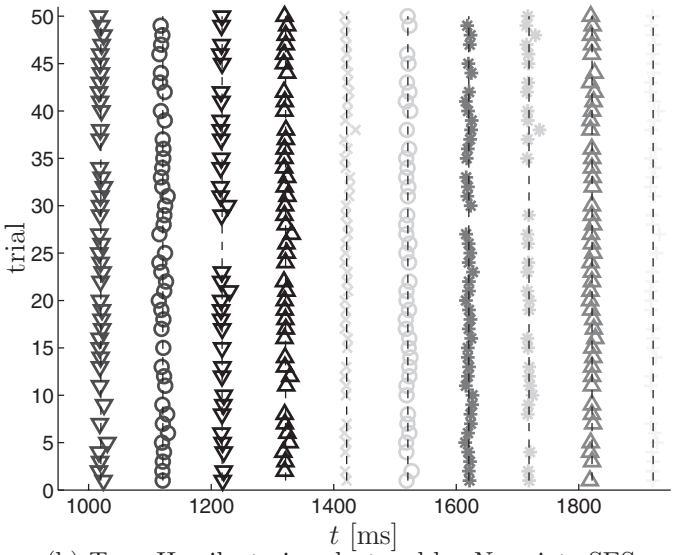

(b) Type II spike trains clustered by N-variate SES.

Figure 11: Results of N-variate SES with $\beta = 10^{-3}$. For clarity, we show the range $t \in [950, 1950]$. Raster plots of spike trains from type I (top) and type II (bottom) neurons. Each cluster is indicated by a different marker type (e.g., star, circle). Background events are marked by hexagons and occur only for the type I neuron.

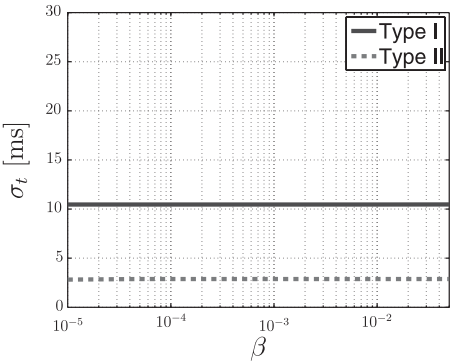

(a) The parameter σ_t as a function of β.

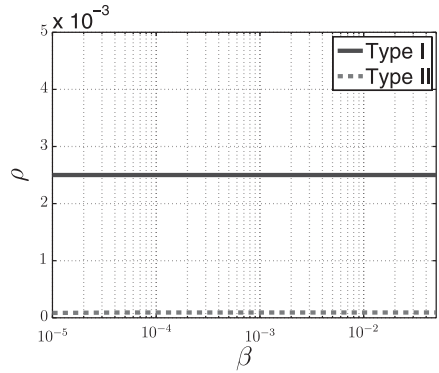

(b) The parameter ρ as a function of β.

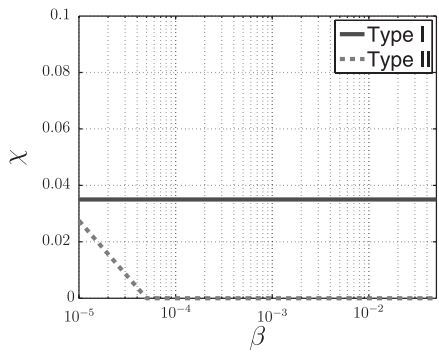

(c) The parameter χ as a function of β.

Figure 12: The parameters σ_t, ρ, and χ estimated from spike trains of type I and type II Morris-Lecar neurons (see Figure 10): the top, middle, and bottom figures show how σ_t, ρ, and χ, respectively, depend on β.

Table 3: Estimates of Bivariate SES Parameters (ρ, σ_t) and N-Variate SES Parameters (ρ, σ_t, χ).

	Bivariate SES		N-Variate SES	
Statistics	Type I	Type II	Type I	Type II
σ_t	10.7	1.91	10.6	2.81
$E[\sigma_t]$	10.8	1.91	10.3	2.87
$\bar{\sigma}[\sigma_t]$	1.8%	1.8%	3.7%	3.0%
ρ	0.0290	0.270	0.0025	0.184
$E[\rho]$	0.0283	0.273	0.0036	0.186
$\bar{\sigma}[\rho]$	12%	3.1%	90%	15%
χ	–	–	0.035	0.0
$E[\chi]$	–	–	0.037	0.0
$\bar{\sigma}[\chi]$	–	–	11%	0.0%

Notes: Also shown are the results from the bootstrapping analysis of those estimates, in particular, the expected values and the normalized standard deviations $\bar{\sigma}$. The expected values practically coincide with the actual estimates and the normalized standard deviations are small; therefore, the estimates may be considered reliable.

actual value, and the normalized standard deviations are small. Therefore, the N-variate SES estimates can be considered reliable.

We first discuss the results for the type I neuron. The estimate of σ_t from bivariate and N-variate SES is almost identical; however, the estimate of ρ is much smaller for N-variate SES than for bivariate SES. Interestingly, N-variate SES inferred that about 3.5% of the events are background events, which accounts for the larger estimate $\rho = 0.029$ from the bivariate approach. In other words, type I neurons almost never fail to fire (firing reliability of 99.75%); however, additional spikes may occur (3.5% of the spikes). It is noteworthy that this insight was obtained by N-variate SES and could not be revealed through bivariate SES. This example thus illustrates that N-variate SES not only yields more accurate estimates of the SES parameters (see section 6), but can also lead to a more refined and detailed analysis. Interestingly, the normalized standard deviation $\bar{\sigma}[\rho]$ is much larger for N-variate SES than for bivariate SES, since ρ is much smaller for N-variate SES. However, the standard deviation $\sigma[\rho]$ is small and about the same for both models.

We now elaborate on the results for the type II neuron. The N-variate approach leads to larger and smaller estimates of σ_t and ρ, respectively, than the bivariate approach. None of the events are considered background events ($\chi = 0$). We have manually counted the number of deletions in Figure 1b and obtained $\rho = 0.184$. The N-variate estimate of ρ is exact and clearly the most reliable, whereas the bivariate approach overestimates the number of deletions. Since the N-variate approach considers all point processes simultaneously ($N = 50$), it infers the hidden process v more

reliably than bivariate SES and is able to associate events x more accurately with hidden events v_k.

We have observed that the N-variate SES algorithm converges after at most three iterations for both type I and type II neurons. In each of those iterations, one updates the decision variables b, c, and e and the SES parameters θ. Since we allowed a maximum number of 30 iterations, we can conclude that the algorithm has always converged in our experiments.

8 Application: Diagnosis of MCI from EEG

Several clinical studies have shown that the EEG of Alzheimer's disease (AD) patients is generally less coherent than of age-matched control subjects; this is also the case for patients suffering from Mild Cognitive Impairment (MCI; see Jeong, 2004; Dauwels et al., 2010b, for a review). In this section, we apply SES to detect subtle perturbations in EEG synchrony of MCI patients. We considered this application also in Dauwels et al. (2009b), where we applied bivariate SES. We analyze here the same EEG data set and use the same preprocessing and bump modeling procedures as in Dauwels et al. (2009b). The only difference is that we here apply N-variate SES instead of bivariate SES.

We first conducted a similar statistical analysis as in Dauwels et al. (2009b). The main results of that analysis are summarized in Figures 13 and 14; they contain p-values obtained by the Mann-Whitney test for the parameters ρ and s_t respectively. This test indicates whether the parameters take different values for the two subject populations. More precisely, low p-values indicate large difference in the medians of the two populations. The p-values are shown for $\hat{\sigma}_t^{(0)} = \sqrt{s_{0,t}} = 0.1, 0.15, \ldots, 0.25$, $\hat{\sigma}_f^{(0)} = \sqrt{s_{0,f}} = 0.05, 0.1, \ldots, 0.15$, $\beta = 0.01, 0.001, 0.0001$, $T = 0.21, 0.22, 0.23$, 0.24, and the number of zones $N_R = 3$ and 5.

The results for the parameters ρ and s_t are quite similar to the results obtained with bivariate SES (see Dauwels et al., 2009b). The lowest p-values for ρ are obtained for $T = 0.22$, $\beta = 0.01$, and $N_R = 5$ (see Figure 13e); the smallest value is $p = 5.4 \cdot 10^{-4}$; in bivariate SES, the smallest p-value ($p = 2.1 \cdot 10^{-4}$) was obtained for $T = 0.22$, $\beta = 0.001$, and $N_R = 5$ (see Dauwels et al., 2009b). As in bivariate SES, the results depend strongly on T (see Dauwels et al., 2009b). (We provided an explanation for this dependency in Dauwels et al., 2009b.) Interestingly, the results depend much less on $\hat{\sigma}_t^{(0)}$, $\hat{\sigma}_f^{(0)}$, and β than in bivariate SES.

From bivariate and N-variate SES analysis (see Figure 13), we can conclude that the statistical differences in ρ are highly significant, especially for $T = 0.22$ and $N_R = 5$. There is a significantly higher degree of noncorrelated activity in MCI patients, more specifically, a high number of noncoincident, nonsynchronous oscillatory events. As in Dauwels et al., (2009b), we did not observe a strongly significant effect on the timing jitter s_t of the

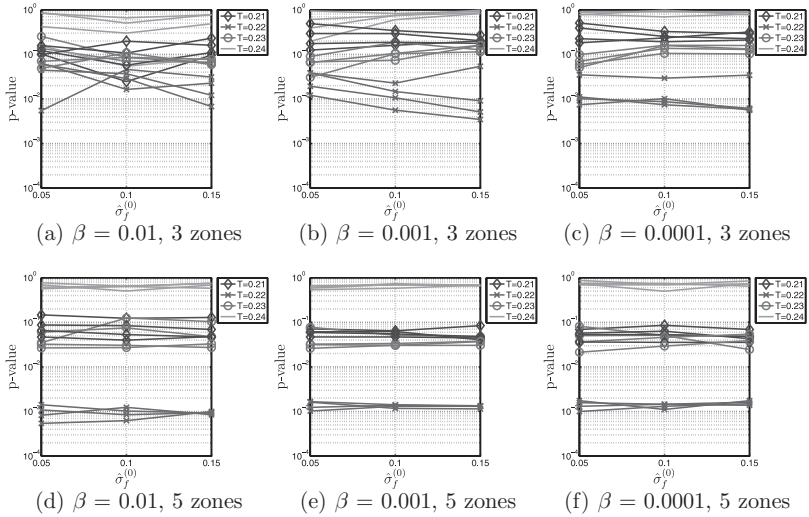

(a) $\beta = 0.01$, 3 zones (b) $\beta = 0.001$, 3 zones (c) $\beta = 0.0001$, 3 zones

(d) $\beta = 0.01$, 5 zones (e) $\beta = 0.001$, 5 zones (f) $\beta = 0.0001$, 5 zones

Figure 13: p-values obtained by the Mann-Whitney test for the parameter ρ for $\hat{\sigma}_t^{(0)} = \sqrt{s_{0,t}} = 0.1, 0.15, \ldots, 0.25$, $\hat{\sigma}_f^{(0)} = \sqrt{s_{0,f}} = 0.05, 0.01, 0.15$, $\beta = 0.01, 0.001, 0.0001$, $T = 0.21, 0.22, 0.23, 0.24$ and the number of zones $N_R = 3$ and 5. The p-values seem to vary little with $\sigma_t^{(0)}$, $\sigma_f^{(0)}$, and β, but are more dependent on T and the number of zones. The lowest p-values are obtained for $T = 0.22$ and $N_R = 5$ zones; the corresponding statistical differences are highly significant.

coincident events (see Figure 14): very few p-values for s_t are smaller than 0.001, which suggests there are no strongly significant differences in s_t.

The N-variate SES model allows us to analyze the results for ρ in more detail. We have investigated how the statistics of bump clusters differ in controls subjects and MCI patients. More specifically, we considered the relative frequency $p_j = p(n_k = j)$ of bump clusters of size $n_k = j$, for $j = 1, 2, \ldots, N_R$. The results are summarized in Figure 15, for the parameter settings that yielded the smallest p-values for ρ ($N_R = 5$ and $\beta = 0.01$). From those figures, we can observe strongly significant differences in clusters of size 1, 2, and 5 for $T = 0.22$; specifically, in MCI patients, there are fewer clusters of sizes 5 and more clusters of sizes 1 and 2. As a result, the fraction of missing events ρ is larger in MCI patients, as we mentioned earlier. The smallest p-value for the parameter p_2 is $p = 2 \cdot 10^{-5}$, which is substantially smaller than the smallest p-value for ρ ($p = 2.1 \cdot 10^{-4}$ for bivariate SES and $p = 5.4 \cdot 10^{-4}$ for N-variate SES).

In Dauwels et al. (2010a) we applied a variety of classical synchrony measures to the same EEG data set. The main results of that analysis are summarized in Table 4. The most significant results were obtained with the full-frequency direct transfer function (ffDTF), a Granger measure

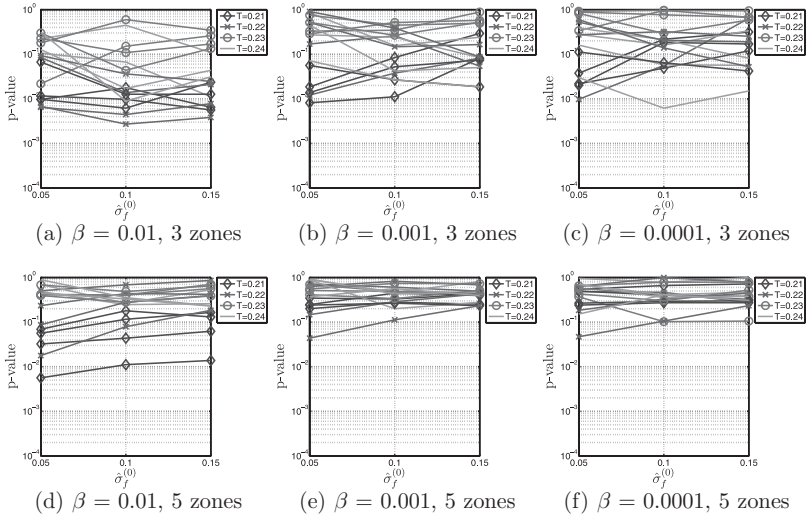

(a) $\beta = 0.01$, 3 zones (b) $\beta = 0.001$, 3 zones (c) $\beta = 0.0001$, 3 zones

(d) $\beta = 0.01$, 5 zones (e) $\beta = 0.001$, 5 zones (f) $\beta = 0.0001$, 5 zones

Figure 14: p-values obtained by the Mann-Whitney test for the parameter s_t for $\hat{\sigma}_t^{(0)} = \sqrt{s_{0,t}} = 0.1, 0.15, \ldots, 0.25$, $\hat{\sigma}_f^{(0)} = \sqrt{s_{0,f}} = 0.05, 0.01, 0.15$, $\beta = 0.01, 0.001, 0.0001$, $T = 0.21, 0.22, 0.23, 0.24$ and the number of zones $N_R = 3$ and 5. Very few p-values are smaller than 0.001, which suggests there are no strongly significant differences in s_t.

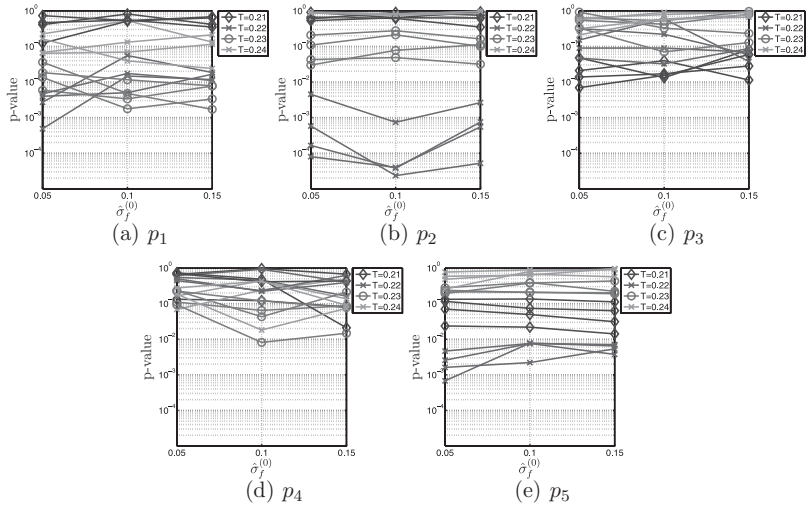

(a) p_1 (b) p_2 (c) p_3

(d) p_4 (e) p_5

Figure 15: p-values obtained by the Mann-Whitney test for the parameters $p_i = p(n_k = i)$ (with $i = 1, 2, \ldots, 5$) for $\hat{\sigma}_t^{(0)} = \sqrt{s_{0,t}} = 0.05, 0.1, 0.15$, $\hat{\sigma}_f^{(0)} = \sqrt{s_{0,f}} = 0.01, 0.15, \ldots, 0.25$, $\beta = 0.01$, $T = 0.22$, and the number of zones $N_R = 5$.

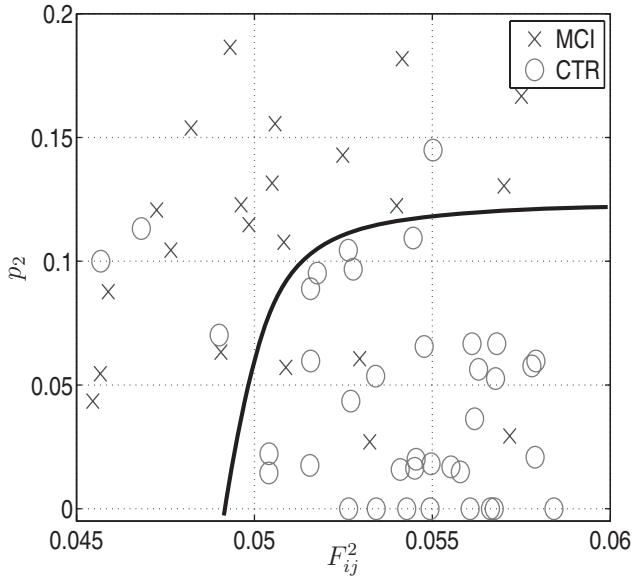

Figure 16: Combining p_2 with ffDTF as features to distinguish MCI from age-matched control subjects. Note that ffDTF is a similarity measure, whereas p_2 is a dissimilarity measure. The (ffDTF, p_2) pairs of the MCI and control subjects tend toward the left top corner and bottom right corner respectively. The smooth curve (solid) yields a classification rate of 87%.

(Pereda et al., 2005), resulting in a p-value of about 10^{-3} (Mann-Whitney test). In Dauwels et al. (2009b), we combined ρ with ffDTF as features to distinguish MCI from control subjects (see Figure 16). About 84% of the subjects are correctly classified. Here we combine ffDTF with the parameter p_2, computed by N-variate SES; the classification rate slightly improves to about 87%. This result is encouraging; however, it is too weak to allow us to predict AD reliably. We would need to combine synchrony measures with complementary statistics, for example, spectral features. We refer to Dauwels et al. (2010b) for more information on potential extensions. Moreover, the results would need to be verified on more data sets.

In summary, N-variate SES helped us to better understand the results from the bivariate SES analysis (Dauwels et al., 2009b): the fraction of missing events ρ is larger in MCI patients, since in those patients, there are fewer bump clusters of sizes 5 and more clusters of sizes 1 and 2. Moreover, N-variate SES allowed us to further improve the classification of MCI patients versus control subjects from 84% to 87%.

Table 4: Sensitivity for Prediction of MCI: Uncorrected p-Values for Mann-Whitney Test.

Measure	Correlation	Coherence	Phase coherence	Corr-entropy	Wave-entropy	
p-value	**0.025***	**0.029***	**0.041***	**0.032***	0.096	
Measure	MVAR coherence	Partial coherence	PDC	DTF	ffDTF	dDTF
p-value	0.15	0.16	0.60	0.29	**0.0012****†	**0.029***
Measure	Kullback-Leibler	Rényi	Jensen-Shannon	Jensen-Rényi	I_W	I
p-value	0.065	0.067	0.069	0.074	0.052	0.060
Measure	N^k	S^k	H^k	S-estimator	Omega complexity	
p-value	**0.029***	**0.045***	0.052	**0.042***	0.079	
Measure	Hilbert phase	Wavelet phase	Evolution map	Instantaneous period	GFS	
p-value	0.96	0.082	0.64	0.73	**0.031***	
Measure	s_t (bivariate)	ρ (bivariate)	s_t (multivariate)	ρ (multivariate)	p_2 (multivariate)	
p-value	0.19	**0.00021****	**0.018***	**0.00054****	$\mathbf{2 \cdot 10^{-5}}$ **	

Notes: * and ** indicate $p < 0.05$ and $p < 0.005$ respectively and those p-values are also shown in bold. † indicates p-values that remain significant after postcorrection. The results for the standard measures and bivariate SES (s_t and ρ) are from Dauwels et al., 2010a, 2009b, respectively, and we refer to those references for more details.

9 Conclusion

We have proposed an approach to determine the similarity of $N > 2$ (one- and multi-dimensional) point processes; it is based on an exemplar-based statistical model that describes how the point processes are related through a common hidden process. The similarity of the point processes is determined by performing inference in that model by means of integer programming techniques in conjunction with point estimation of the parameters. The proposed technique may be used for various applications in neuroscience (e.g., in brain-computer interfaces, analysis of spike data), biomedical signal processing, and beyond.

In bivariate SES, we apply the max-product algorithm for aligning pairs of sequences. As we have observed, this algorithm performs poorly for aligning $N > 2$ sequences. We have also experimented with various refinements of the max-product algorithm, and none of them yielded satisfactory results. An interesting topic for future research is to develop extensions of the max-product algorithm that lead to optimal or close-to-optimal N-wise alignments. Such message-passing algorithms are often simpler and faster than integer linear programming techniques.

Appendix A: Derivation of the SES Model

In this appendix, we derive the N-variate SES model, equation 3.17.

We first marginalize $p(x, c, v, \theta, \ell)$, equation 3.16, over v; it is noteworthy that only the gaussian terms $\mathcal{N}(\cdot)$ in equation 3.16 depend on v. In the following, we focus on those terms. For a given hidden event v_k, three cases are possible:

- *All* copies of v_k were deleted ($n_k = 0$). There are no gaussian terms associated with v_k in equation 3.16. Therefore, the expression may be considered as constant with regard to v_k. Integrating this equation over v_k then leads to a term $\mathrm{vol}(S)$. There are L^{del} such terms, since the number of hidden events v_k without copies is given by L^{del}.
- There is one copy of v_k ($n_k = 1$), and therefore only one gaussian term in equation 3.16 that corresponds to v_k. Integrating that term over v_k results in the (trivial) term 1.
- There is more than one copy of v_k ($n_k > 1$), and as a consequence, several gaussian terms in equation 3.16 correspond to v_k. As can be easily shown, integrating the n_k gaussian terms over v_k yields these terms:

$$\prod_{(i,j)\in\mathcal{I}_k} \mathcal{N}\big(t_{ij} - \bar{t}_k; \delta_{ti}, s_{ti}\big)\, \mathcal{N}\big(f_{ij} - \bar{f}_k; \delta_{fi}, s_{fi}\big), \tag{A.1}$$

where

$$\bar{t}_k = \frac{\sum_{(i,j)\in\mathcal{I}_k} w_{ti}(t_{ij} - \delta_{ti})}{\sum_{(i,j)\in\mathcal{I}_k} w_{ti}} \tag{A.2}$$

$$\bar{f}_k = \frac{\sum_{(i,j)\in\mathcal{I}_k} w_{fi}(f_{ij} - \delta_{fi})}{\sum_{(i,j)\in\mathcal{I}_k} w_{fi}}, \tag{A.3}$$

with $w_{ti} = s_{ti}^{-1}$ and $w_{fi} = s_{fi}^{-1}$.

In summary, marginalizing over v results in L^{del} terms $\text{vol}(S)$, and also in terms of the form A.1, where there is one such term for each cluster of size $n_k > 1$.

The result of marginalizing over v may then be written as

$$\begin{aligned} p(x, c, \theta, \ell) &\propto p(s_t)p(s_f)(1 - \lambda\,\text{vol}(S))(\lambda\text{vol}(S)p_d^N)^{L^{\text{del}}} \\ &\cdot(\lambda p_d^N)^L p_d^{-L^{\text{tot}}}(1 - p_d)^{L^{\text{tot}}} \\ &\cdot \prod_{k\in\mathcal{K}} \prod_{(i,j)\in\mathcal{I}_k} \mathcal{N}\big(t_{ij} - \bar{t}_k; \delta_{ti}, s_{ti}\big)\,\mathcal{N}\big(f_{ij} - \bar{f}_k; \delta_{fi}, s_{fi}\big), \end{aligned} \tag{A.4}$$

where we used the decomposition

$$\ell = L + L^{\text{del}}. \tag{A.5}$$

Now we marginalize over the length ℓ. The first term in the decomposition, equation A.5, is fixed for given clustering c. Therefore, marginalizing $p(x, c, \theta, \ell)$ A.4 over ℓ is equivalent to marginalizing over L^{del}:

$$p(x, c, \theta) = \sum_{\ell=0}^{\infty} p(x, c, \theta, \ell) = \sum_{L^{\text{del}}=0}^{\infty} p(x, c, \theta, \ell) \tag{A.6}$$

$$\begin{aligned} &\propto p(s_t)p(s_f)(1 - \lambda\,\text{vol}(S)) \sum_{L^{\text{del}}=0}^{\infty} \big(\lambda\text{vol}(S)p_d^N\big)^{L^{\text{del}}} \\ &\cdot\big(\lambda p_d^N\big)^L p_d^{-L^{\text{tot}}}(1 - p_d)^{L^{\text{tot}}} \\ &\cdot \prod_{k\in\mathcal{K}} \prod_{(i,j)\in\mathcal{I}_k} \mathcal{N}\big(t_{ij} - \bar{t}_k; \delta_{ti}, s_{ti}\big)\,\mathcal{N}\big(f_{ij} - \bar{f}_k; \delta_{fi}, s_{fi}\big) \end{aligned} \tag{A.7}$$

$$\begin{aligned} &\propto p(s_t)p(s_f)(1 - \lambda\,\text{vol}(S))\frac{1}{1 - \lambda\text{vol}(S)p_d^N} \\ &\cdot(\lambda p_d^N)^L p_d^{-L^{\text{tot}}}(1 - p_d)^{L^{\text{tot}}} \\ &\cdot \prod_{k\in\mathcal{K}} \prod_{(i,j)\in\mathcal{I}_k} \mathcal{N}\big(t_{ij} - \bar{t}_k; \delta_{ti}, s_{ti}\big)\,\mathcal{N}\big(f_{ij} - \bar{f}_k; \delta_{fi}, s_{fi}\big). \end{aligned} \tag{A.8}$$

A sum of a geometric series occurs in equation A.7. Since $|\lambda \mathrm{vol}(S) p_d^N| = \lambda \mathrm{vol}(S) p_d^N < 1$, we can apply the well-known formula for the sum of a geometric series, resulting in equation A.8. By defining β and γ as in equations 3.20 and 3.21, respectively, we obtain statistical model 3.17.

Appendix B: Derivation of the SES Inference Algorithm

In this appendix, we derive the inference update, equation 4.3, for N-variate SES.

The point estimates $\hat{\delta}_{ti}^{(\kappa)}$ and $\hat{\delta}_{fi}^{(\kappa)}$ are the (sample) mean of the timing and frequency offset, respectively, computed between all events in x_{ij} and their associated cluster centers:

$$\hat{\delta}_{ti}^{(\kappa)} = \frac{1}{L_i} \sum_{j=1}^{L_i} \left(t_{ij} - \bar{t}_{\hat{c}_{ij}^{(\kappa)}} \right), \tag{B.1}$$

$$\hat{\delta}_{fi}^{(\kappa)} = \frac{1}{L_i} \sum_{j=1}^{L_i} \left(f_{ij} - \bar{f}_{\hat{c}_{ij}^{(\kappa)}} \right), \tag{B.2}$$

where L_i is the number of events in x_i and $\bar{t}_{\hat{c}_{ij}^{(\kappa)}}$ and $\bar{f}_{\hat{c}_{ij}^{(\kappa)}}$ are the coordinates of the (inferred) hidden event $v_{\hat{c}_{ij}^{(\kappa)}}$ associated with x_{ij}. The latter hidden event is inferred as the center of the cluster associated with x_{ij}. The coordinates $\bar{t}_k$ and $\bar{f}_k$ are computed as

$$\bar{t}_k = \frac{\sum_{(i,j) \in \hat{\mathcal{I}}_k^{(\kappa)}} \hat{w}_{ti}^{(\kappa)} (t_{ij} - \hat{\delta}_{ti}^{(\kappa)})}{\sum_{(i,j) \in \hat{\mathcal{I}}_k^{(\kappa)}} \hat{w}_{ti}^{(\kappa)}}, \tag{B.3}$$

$$\bar{f}_k = \frac{\sum_{(i,j) \in \hat{\mathcal{I}}_k^{(\kappa)}} \hat{w}_{fi}^{(\kappa)} (f_{ij} - \hat{\delta}_{fi}^{(\kappa)})}{\sum_{(i,j) \in \hat{\mathcal{I}}_k^{(\kappa)}} \hat{w}_{fi}^{(\kappa)}}, \tag{B.4}$$

with $\hat{w}_{ti}^{(\kappa)} = \left(\hat{s}_{ti}^{(\kappa)} \right)^{-1}$, $\hat{w}_{fi}^{(\kappa)} = \left(\hat{s}_{fi}^{(\kappa)} \right)^{-1}$, and $\hat{\mathcal{I}}_k^{(\kappa)}$ is the index set of the set $\hat{\mathcal{C}}_k^{(\kappa)}$ of events in cluster k (as specified by $\hat{c}^{(\kappa)}$):

$$\mathcal{C}_k^{(\kappa)} = \left\{ x_{ij} : \hat{c}_{ij}^{(\kappa)} = k \right\} \text{ and } \mathcal{I}_k^{(\kappa)} = \left\{ (i, j) : \hat{c}_{ij}^{(\kappa)} = k \right\}. \tag{B.5}$$

The estimates $\hat{s}_{ti}^{(\kappa)}$ and $\hat{s}_{fi}^{(\kappa)}$ are obtained as

$$\hat{s}_{ti}^{(\kappa)} = \frac{\nu_t s_{t0} + L_i \hat{s}_{ti,\text{sample}}^{(\kappa)}}{\nu_t + L_i + 2}, \tag{B.6}$$

$$\hat{s}_{fi}^{(\kappa)} = \frac{\nu_f s_{f0} + L_i \hat{s}_{fi,\text{sample}}^{(\kappa)}}{\nu_f + L_i + 2}, \tag{B.7}$$

where $s_{ti,\text{sample}}^{(\kappa)}$ and $s_{fi,\text{sample}}^{(\kappa)}$ are computed as

$$\hat{s}_{ti,\text{sample}}^{(\kappa)} = \frac{1}{L_i} \sum_{j=1}^{L_i} \left(t_{ij} - \bar{t}_{\hat{c}_{ij}^{(\kappa)}} - \hat{\delta}_{ti}^{(\kappa)} \right)^2 \tag{B.8}$$

$$\hat{s}_{fi,\text{sample}}^{(\kappa)} = \frac{1}{L_i} \sum_{j=1}^{L_i} \left(f_{ij} - \bar{f}_{\hat{c}_{ij}^{(\kappa)}} - \hat{\delta}_{fi}^{(\kappa)} \right)^2, \tag{B.9}$$

and where $\bar{t}_k$ and $\bar{f}_k$ are given by equations B.3 and B.4.

Interestingly, the right-hand side of equations B.1 and B.2 depends on $\hat{\delta}_{ti}^{(\kappa)}$ and $\hat{\delta}_{fi}^{(\kappa)}$, respectively, through equations B.3 and B.4. Therefore the equalities B.1 and B.2 need to be solved numerically; the same holds for equations B.6 and B.7. Those expressions may be evaluated numerically by alternating the updates, equations B.3 and B.4 with B.1, B.2, B.6, and B.7 with, as initial estimates, $\hat{\delta}_{ti}^{(\kappa-1)}$, $\hat{\delta}_{fi}^{(\kappa-1)}$, $\hat{s}_{ti}^{(\kappa-1)}$, and $\hat{s}_{fi}^{(\kappa-1)}$. It can easily be shown that this procedure is guaranteed to converge to a local extremum; indeed, it is equivalent to cyclic maximization, where one conditional maximization is in θ (resulting in equations B.1, B.2, B.6, and B.7), and the other is in the parameters $\{(\bar{t}_k, \bar{f}_k)\}_{k=1,\ldots,L}$ (resulting in equations B.3 and B.4).

Acknowledgments

We thank the anonymous reviewers for their helpful feedback, which substantially improved the letter. Part of this work was carried out while J.D. was at the Laboratory for Information and Decision Systems, MIT, Cambridge, MA.

References

Abeles, M., Bergman, H., Margalit, E., & Vaadia, E. (1993). Spatiotemporal firing patterns in the frontal cortex of behaving monkeys. *J. Neurophysiol.*, *70*(4), 1629–1638.

Amari, S., Nakahara, H., Wu, S., & Sakai, Y. (2003). Synchronous firing and higher-order interactions in neuron pool. *Neural Computation*, *15*, 127–142.

Buzsáki, G. (2006). *Rhythms of the brain*. New York: Oxford University Press.

Dauwels, J., Tsukada, Y., Sakumura, Y., Ishii, S., Aoki, K., Nakamura, T., et al. (2008). On the synchrony of morphological and molecular signaling events in cell migration. In *Proceedings of the International Conference on Neural Information Processing* (pp. 469–477). Berlin: Springer-Verlag.

Dauwels, J., Vialatte, F., & Cichocki, A. (2010a). A comparative study of synchrony measures for the early diagnosis of Alzheimer's disease based on EEG. *Neuroimage*, *49*, 668–693.

Dauwels, J., Vialatte, F., & Cichocki, A. (2010b). Diagnosis of Alzheimer's disease from EEG signals: Where are we standing? *Curr. Alzheimer Research*, Epub May 11 2010.

Dauwels, J., Vialatte, F., Rutkowski, T., & Cichocki, A. (2008). Measuring neural synchrony by message passing. In J. Platt, D. Koller, Y. Singer, & S. Roweis (Eds.), *Advances in neural information processing systems*, 20 (pp. 361–368). Cambridge, MA: MIT Press.

Dauwels, J., Vialatte, F., Weber, T., & Cichocki, A. (2009a). Quantifying statistical interdependence by message passing on graphs: I. One-dimensional point processes. *Neural Computation*, *21*(8), 2152–2202.

Dauwels, J., Vialatte, F., Weber, T., & Cichocki, A. (2009b). Quantifying statistical interdependence by message passing on graphs: II. Multi-dimensional point processes. *Neural Computation*, *21*(8), 2203–2268.

Efron, B., & Tibshirani, R. (1993). *An introduction to the bootstrap*. London: Chapman & Hall/CRC.

Frey, B., & Dueck, D. (2007). Clustering by passing messages between data points. *Science*, *315*(5814), 972–976.

Givoni, I., & Frey, B. J. (2009). A binary variable model for affinity propagation. *Neural Computation*, *21*, 1589–1600.

Gutkin, B. S., & Ermentrout, G. B. (1998). Dynamics of membrane excitability determine interspike interval variability: A link between spike generation mechanisms and cortical spike train statistics. *Neural Computation*, *10*, 1047–1065.

Jeong, J. (2004). EEG dynamics in patients with Alzheimer's disease. *Clinical Neurophysiology*, *115*, 1490–1505.

Lashkari, D., & Golland, P. (2008). Convex clustering with exemplar-based models. In J. Platt, D. Koller, Y. Singer, & S. Roweis (Eds.), *Advances in neural information processing systems*, *20* (pp. 361–368). Cambridge, MA: MIT Press.

Matsuda, H. (2001). Cerebral blood flow and metabolic abnormalities in Alzheimer's disease. *Ann. Nucl. Med.*, *15*, 85–92.

Morris, C., & Lecar, H. (1981). Voltage oscillations in the barnacle giant muscle fiber. *Biophys. J.*, *35*, 193–213.

Nunez, P., & Srinivasan, R. (2006). *Electric fields of the brain: The neurophysics of EEG*. New York: Oxford University Press.

Pereda, E., Quiroga, R. Q., & Bhattacharya, J. (2005). Nonlinear multivariate analysis of neurophysiological signals. *Progress in Neurobiology*, *77*, 1–37.

Quiroga, R. Q., Kraskov, A., Kreuz, T., & Grassberger, P. (2002). Performance of different synchronization measures in real data: A case study on EEG signals. *Physical Review E*, *65*.

Robinson, H.P.C. (2003). The biophysical basis of firing variability in cortical neurons. In J. Feng (Ed.), *Computational neuroscience: A comprehensive approach*. London: Chapman & Hall/CRC.

Singer, W. (2001). Consciousness and the binding problem, 2001. *Annals of the New York Academy of Sciences*, *929*, 123–146.

Stam, C. J. (2005). Nonlinear dynamical analysis of EEG and MEG: Review of an emerging field. *Clinical Neurophysiology*, *116*, 2266–2301.

Tateno, T., & Pakdaman, K. (2004). Random dynamics of the Morris-Lecar neural model. *Chaos*, *14*(3).

Toups, J., Fellous, J.-M., Thomas, P., Sejnowski, T., & Tiesinga, P. (2011). Finding the event structure of neuronal spike trains. *Neural Computation*, *23*(9), 2169–2208.

Tsumoto, K., Kitajima, H., Yoshinaga, T., Aihara, K., & Kawakami, H. (2006). Bifurcations in Morris-Lecar neuron model. *Neurocomputing*, *69*, 293–316.

Varela, F., Lachaux, J. P., Rodriguez, E., & Martinerie, J. (2001). The brainweb: Phase synchronization and large-scale integration. *Nature Reviews Neuroscience*, *2*(4), 229–239.

Vialatte, F., Martin, C., Dubois, R., Haddad, J., Quenet, B., Gervais, R., et al. (2007). A machine learning approach to the analysis of time-frequency maps, and its application to neural dynamics. *Neural Networks*, *20*, 194–209.

Victor, J. D., & Purpura, K. P. (1997). Metric-space analysis of spike trains: Theory, algorithms, and application. *Network: Comput. Neural Systems*, *8*(17), 127–164.

Womelsdorf, T., Schoffelen, J. M., Oostenveld, R., Singer, W., Desimone, R., Engel, A. K., et al. (2007). Modulation of neuronal interactions through neuronal synchronization. *Science*, *316*, 1609–1612.

Received January 1, 2011; accepted August 20, 2011.

This article has been cited by: